ELSEVIER

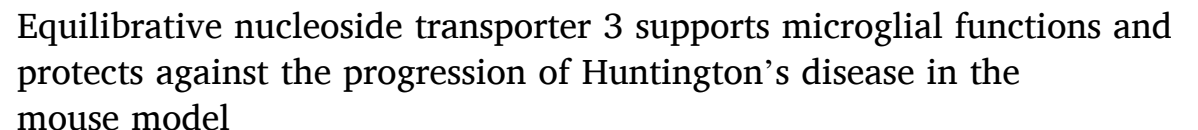
Contents lists available at ScienceDirect

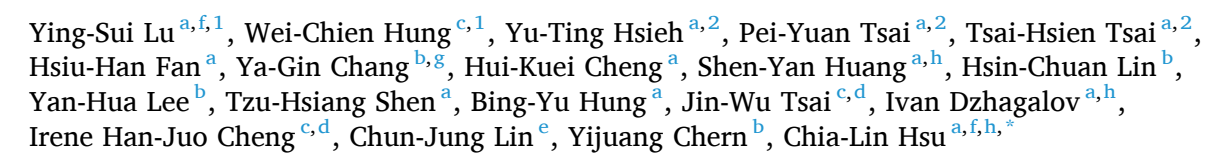
## Brain Behavior and Immunity

journal homepage: www.elsevier.com/locate/ybrbi



## Full-length Article





- <sup>a</sup> Institute of Microbiology and Immunology, National Yang Ming Chiao Tung University, Taipei, Taiwan
- <sup>b</sup> Institute of Biomedical Sciences, Academia Sinica, Taipei, Taiwan
- <sup>c</sup> Institute of Brain Science, National Yang Ming Chiao Tung University, Taipei, Taiwan
- <sup>d</sup> Brain Research Center, National Yang Ming Chiao Tung University, Taipei, Taiwan
- e School of Pharmacy, College of Medicine, National Taiwan University, Taipei, Taiwan
- f Taiwan International Graduate Program in Molecular Medicine, National Yang Ming Chiao Tung University and Academia Sinica, Taipei, Taiwan
- g Taiwan International Graduate Program in Interdisciplinary Neuroscience, National Yang Ming Chiao Tung University and Academia Sinica, Taipei, Taiwan
- h Biomedical Industry Ph.D. Program, National Yang Ming Chiao Tung University, Taipei, Taiwan

#### ABSTRACT

Huntington's disease (HD) is a hereditary neurodegenerative disorder characterized by involuntary movements, cognitive deficits, and psychiatric symptoms. Currently, there is no cure, and only limited treatments are available to manage the symptoms and to slow down the disease's progression. The molecular and cellular mechanisms of HD's pathogenesis are complex, involving immune cell activation, altered protein turnover, and disturbance in brain energy homeostasis. Microglia have been known to play a dual role in HD, contributing to neurodegeneration through inflammation but also enacting neuroprotective effects by clearing mHTT aggregates. However, little is known about the contribution of microglial metabolism to HD progression. This study explores the impact of a microglial metabolite transporter, equilibrative nucleoside transporter 3 (ENT3), in HD. Known as a lysosomal membrane transporter protein, ENT3 is highly enriched in microglia, with its expression correlated with HD severity. Using the R6/2 ENT3<sup>-/-</sup> mouse model, we found that the deletion of ENT3 increases microglia numbers yet worsens HD progression, leading to mHTT accumulation, cell death, and disturbed energy metabolism. These results suggest that the delicate balance between microglial metabolism and function is crucial for maintaining brain homeostasis and that ENT3 has a protective role in ameliorating neurodegenerative processes.

### 1. Introduction

Huntington's disease (HD) is a progressive neurodegenerative disorder that primarily affects the central nervous system (CNS). As an inherited autosomal disease, this debilitating condition is characterized by a range of involuntary movements, cognitive deficits, and psychiatric symptoms. HD is caused by the monogenic disorder of expanded CAG repeats in the huntingtin (Htt) gene (Tabrizi et al., 2020), leading to the accumulation of mutant huntingtin (mHTT). The mHTT protein undergoes abnormal folding, leading to the formation of protein aggregates within the cells. These aggregates interfere with essential cellular

processes, impairing neuronal function and survival, and are positively correlated with massive neuronal cell death and degeneration. The striatum, a brain region involved in motor control, is affected particularly severely in HD. Currently, there is no cure for HD, with only limited treatment strategies available to manage the symptoms and slow down disease progression.

Although HD has a well-defined genetic origin, the molecular and cellular mechanisms underlying the pathogenesis of HD are complex. While aggregate formation and toxic fragment production lead to cellular transcriptional deregulation, altered protein homeostasis, and mitochondrial dysfunction, neuroglial disturbance, such as

<sup>\*</sup> Corresponding author at: Institute of Microbiology and Immunology, National Yang Ming Chiao Tung University, Taipei, Taiwan. E-mail address: clhsu@nycu.edu.tw (C.-L. Hsu).

<sup>&</sup>lt;sup>1</sup> Co-first author.

<sup>&</sup>lt;sup>2</sup> These authors contribute equally.

neuroinflammation and impaired glutamate uptake by astrocytes, is another crucial contributor to HD pathophysiology (Jimenez-Sanchez et al., 2017). Interestingly, the neuroinflammation and the protein-degradation-resultant defects such as autophagic-lysosomal dysfunction in HD are shared features with other neurological diseases such as Alzheimer's disease (AD) or lysosomal storage diseases (LSDs). The majority of LSDs present different degrees of pathology in the CNS and neurodegeneration in multiple brain regions. Depending on the specific type of metabolite accumulation, the patients vary in affected age or neuronal subtypes (Platt et al., 2012). The commonality between these diseases suggests a potential shared molecular mechanism caused by abnormal protein aggregation, autophagic-lysosomal dysfunction, and neuroinflammation.

Microglia, brain resident macrophages, are the major immune cell population contributing to brain homeostasis via phagocytosis, scavenging activity, and cytokine secretion. In addition to rapidly initiating innate immune responses upon insult, microglia also play a vital part in tissue repair and regeneration (Lukens & Eyo, 2022). On the other hand, dysregulated microglia can lead to chronic inflammation, tissue damage, and furthered disease progression (Muzio et al., 2021). In the context of HD, microglia are activated in response to the presence of mHTT and the subsequent production and release of pro-inflammatory molecules, examples being cytokines, chemokines, and reactive oxygen species (Palpagama et al., 2019). This inflammatory response can exacerbate neurodegenerative processes by causing oxidative stress, promoting excitotoxicity, and initiating a cascade of damaging events (Wilton & Stevens, 2020). However, microglia also exert neuroprotective effects in HD. They are involved in clearing mHTT aggregates and cellular debris through phagocytosis. Microglia can engulf and remove toxic protein aggregates, contributing to maintaining brain homeostasis (Gao et al., 2023). During the process of removing unwanted substances and degrading engulfed material, microglia play several roles in recycling valuable metabolites and initiating repairing immune response, or in inducing neuroinflammation from both extrinsic or cellautonomous mechanisms (Colonna & Butovsky, 2017). However, the direct effects of the accumulated metabolite itself or the disturbance of metabolite equilibrium on the activity and function of microglia remain largely unknown.

Energy consumption and associated metabolic processes are highly dynamic in the brain. The shifts of metabolic programs happen constantly to support neuronal functions. Energy is primarily produced through cellular respiration, which involves the breakdown of glucose and other molecules in the mitochondria. In HD, there is evidence of impaired energy metabolism in brain cells (Dubinsky, 2017) (Mochel & Haller, 2011). Metabolites, such as adenosine, that exist both intracellularly and extracellularly, can affect many crucial biochemical processes, including energy generation/consumption, cell signal transduction, and DNA/RNA synthesis. Given its biological importance, the extracellular and intracellular amounts of adenosine are tightly regulated by a group of proteins: ecto-nucleotidases CD39 and CD73, adenosine deaminase (ADA), adenosine kinase (ADK), and adenosine transporters such as equilibrative nucleoside transporters (ENTs). ENTs are encoded by the solute carrier family 29 (SLC29) gene; ENTs 1 to 4 are transmembrane proteins that facilitate the transport of nucleosides and nucleobases among cellular spaces. Previously, we identified ENT3 as an essential intracellular transporter regulating lysosomal function, with a deficiency of ENT3 impacting the function and homeostasis of macrophages (Hsu et al., 2012). Although ENT3 mutations have been associated with a broad spectrum of diseases (Ma et al., 2023), the pathophysiological roles of ENT3 in neurodegenerative diseases have not been explored.

In this study, we found ENT3 is the nucleoside transporter that is highly expressed in microglia, with the deletion of ENT3 leading to an increased number of microglia in the brain. Under a disease setting, the elevated expression of *SLC29A3* in HD patients is likely a reflection of its functional demand in microglia to process the mHTT aggregates. The deficiency of ENT3 leads to the worsening of HD progression,

accumulation of mHTT in the striatum and cell death, as well as the eventual disturbed energy metabolism in the R6/2 disease mouse model. The R6/2 ENT3 $^{-/-}$  microglia experience high oxidative stress and lose lysosomal integrity. We reveal that ENT3 not only participates in the homeostasis of the microglia population but is also involved in the protective microglial function during the HD setting.

#### 2. Materials and methods

## 2.1. Mice

Wild-type (WT) mice were obtained from Taiwan's National Laboratory Animal Center. ENT3<sup>-/-</sup> mice were imported from the mutant mouse regional resource center (MMRRC) (Tang et al., 2010). Cx3cr1-GFP knock-in mice [B6.129P2(Cg)-Cx3cr1tm1Litt/J] and R6/2 (B6CBA-Tg(HDexon1)62Gpb/1J) strains were obtained from Jackson Laboratories (Bar Harbor, ME, USA). ROSA26<sup>GFP</sup> strain was generated at the Dzhagalov lab. To obtain Cx3cr1<sup>GFP/+</sup>ENT3<sup>-/-</sup> mice, Cx3cr1<sup>GFP/+</sup> was crossed with ENT3<sup>+/-</sup> to generated Cx3cr1<sup>GFP/+</sup> ENT3<sup>+/-</sup> mice. The resulting Cx3cr1<sup>GFP/+</sup> ENT3<sup>+/-</sup> was then crossed with ENT3<sup>+/-</sup> Cx3cr1<sup>GFP/+</sup>ENT3<sup>-/-</sup> mice and their littermate controls Cx3cr1<sup>GFP/</sup> <sup>+</sup>ENT3<sup>+/+</sup> were used for the experiments. For the R6/2<sup>+/-</sup>ENT3<sup>-/-</sup> strain, male ENT3<sup>+/-</sup> on C57BL/6 (B6) background was mated with female CBA (CBA/CaJNarl) mice to produce CBA/B6-ENT3<sup>+/-</sup> mice. The female mixed background CBA/B6-ENT3<sup>+/-</sup> mice were crossed with male R6/2 mice to generate R6/2<sup>+/-</sup>ENT3<sup>+/-</sup> mice. The male R6/  $2^{+/-}$ ENT3 $^{+/-}$  then was crossed with female CBA/B6-ENT3 $^{+/-}$  to generate  $R6/2^{+/-}$  ENT3 $^{-/-}$  and their littermate controls  $R6/2^{+/-}$ ENT3<sup>+/+</sup> were used for the experiments. The number of CAG repeats was 233.0  $\pm$  14 for the R6/2 mice used in this study. Mice were genotyped and housed at the Institute of Biomedical Sciences Animal Care Facility at Academia Sinica or Laboratory Animal Center at NYCU (Taipei, Taiwan) under a 12-h light/dark cycle. The number of CAG repeats was 233.0  $\pm$  14 for the R6/2 mice used in this study. All animal experiments were performed under protocols approved by the Academia Sinica and NYCU Institutional Animal Care and Utilization Committee.

## 2.2. Isolation of astrocytes, microglia, and neurons from adult mouse brains for SLC family transcript quantification

Brain cells were isolated from adult R6/2 mice and their littermate controls at seven weeks old. The mice were perfused with 0.9 % NaCl to remove blood cells. The cerebral cortex was carefully removed from the skull, diced into small pieces, and dissociated by enzymatic digestion (MACS, #130-092-628) and triturated with glass pipets (1.0, 0.75, and 0.5 mm in diameter). Cell debris and myelin were removed by Percoll density centrifugation at 650  $\times$  g for 25 min at room temperature (dissociated cells were prepared in 30 % Percoll and loaded onto 70 % Percoll prepared in Mg<sup>2+</sup> and Ca<sup>2+</sup>-free HBSS), and myelin removal beads II (MACS, #30-096-733). Magnetic beads conjugated to anti-ACSA2 (MACS, #130-092-678) or anti-CD11b (MACS, #130-093-634) were used to isolate astrocytes and microglia sequentially. The isolated cells were eluted and kept in liquid nitrogen until RNA extraction. A biotin-labeled nonneuronal antibody cocktail (MACS, #130-115-390) and magnetic beads conjugated to the anti-biotin antibody were used to isolate neurons. The unlabeled cells (i.e., neurons) were isolated using an LS column placed on a magnetic separator and kept in liquid nitrogen until RNA extraction. The total RNA of isolated cells was extracted using the PureLink RNA Micro kit (Invitrogen, #12183-016). The quality of the isolated RNA was evaluated using an Agilent bioanalyzer 2100 with a bioanalyzer RNA 6000 Pico chip. Only the RNA with an RNA Integrity Number (RIN) higher than seven was used for further amplification and cDNA synthesis by the Ovation® PicoSL WTA system V2 (Nugene, #3312).

The copy numbers of each SLC29 family member (slc29a1, slc29a, slc29a3, and slc29a4) in isolated microglia were calculated using

absolute quantitative PCR given with a standard curve for specific ENT subtypes. Each standard curve for corresponding genes was established by 10-fold serial dilutions of purified plasmid expressing indicated ENT subtypes. The DNA concentrations against their corresponding Ct values are used to quantify the target transcript. Copy number was calculated using the following equation: Copy number = [(DNA concentration)  $\times$  (Avogadro constant)] / [(length of DNA fragment)  $\times$  (average weight of a double-stranded base pair)].

## 2.3. Modified SmithKline, Harwell, Imperial College, Royal Hospital, phenotype assessment (SHIRPA)

Ten- to twelve-week-old ENT3<sup>-/-</sup> and littermate mice (male and female ratio 1:1) were subjected to the modified SHIRPA test. The modified SHIRPA test consists of 58 items, including 33 behavioral observations, seven metabolic or disease observations, two additional notes on behavior, and 16 criteria used to screen for abnormalities in animal growth, development, or metabolism. These tests were used for the initial analysis of experimental animal behavior and to assess whether there are behavioral abnormalities caused by muscle, motor nerve, spinal cerebellar, sensory central, or autonomic nervous system disorders (Masuya et al., 2005).

## 2.4. Open field test

The open field test was performed as previously described (Liu et al., 2017). To detect the spontaneous locomotor activity, the individual mouse was placed in an open chamber ( $24.32 \times 24.32 \, \mathrm{cm}^2$ ) and allowed to explore freely for 15 min. The movement track was detected by  $16 \times 16$  infrared photo-beam arrays placed 1.5 cm above the bottom of the chamber (Version 2.0, TRU Scan Photobeam LINC, Coulbourn Instruments, PA, USA). Margin time is defined as the total time spent within a 2.5-beam margin of the walls.

## 2.5. Wire hang test

The wire hang test was performed as follows: The mouse was placed in the center of the wire mesh (10 cm² consisting of 2 mm squares), which was then inverted for 3 min. The wire mesh was positioned at a stage 40 cm above the soft bedding material. If the mouse fell off, the time was recorded. This test was performed three days per week with three trials per session. The average performance for each session is presented as the average of the three trials (Aartsma-Rus & van Putten, 2014).

## 2.6. Elevated maze test

The test was performed as described previously (Lee et al., 2021). The elevated maze apparatus contains two open arms and two closed arms. At the beginning of the test, the mice were placed in the center of the maze and faced the closed arm. The mice were then allowed to explore freely for 10 min. During the test period, their movements were recorded by the camera and analyzed with the EthoVision video tracking system (Version 3.1 Noldus Wageningen, Netherlands).

## 2.7. Flow cytometric analysis

To avoid undesirable removal of surface proteins during the enzymatic isolation procedure, the surface marker profiling of microglia was performed by mechanical homogenization, as described below. Mice were anesthetized and perfused with 0.1 M PBS buffer before brains were quickly dissected and minced by scalpels on ice ground with a plastic homogenizer in ice-cold Hank's balanced salt solution (HBSS without  $Mg^{2+}$ ,  $Ca^{2+}$ ,  $Gibco^{TM}$ , #14175095). The resulting tissue homogenate was filtered through a 70  $\mu$ m strainer (Biologix, #15-1070) and subsequently centrifuged at 300  $\times$  g for 15 min at 18 °C, and the

supernatant was removed. Debris and myelin were removed using a stock isotonic Percoll (Sigma-Aldrich, #17-5445-01) (SIP) gradient. Cell pellets were resuspended in 10 mL of 30 % SIP underlaid with 3 mL 70 % SIP and centrifuged at 650  $\times$  g without breaks for 25 min at room temperature. The interface was collected and washed with 10 mL of ice-cold HBSS and spun again for 10 min at 300  $\times$  g at 4  $^{\circ}$ C. The cell pellets were re-suspended in 100 uL of FACS buffer for subsequent antibody staining.

The sample was first incubated on ice with supernatant from 2.4G2 hybridoma for 20 min to block Fc receptors. After blocking, the fluorescence-conjugated antibodies combo prepared in FACS buffer (1 mM EDTA, 5 % FBS in 0.1 M PBS buffer) was added to the sample and kept on ice in the dark for 20 min. The following antibodies were used in this study: CD11b (BioLegend, #101206) (BioLegend, #101251), CD45 (BioLegend, #103128), CD206 (BioLegend, #141706), Tim4 (BioLegend, #130010), MHC II (BioLegend, #107652), CD80 (BioLegend, #104729), CD86 (BioLegend, #105036). The cells were washed twice in PBS, resuspended in a pre-chilled FACS buffer containing propidium iodide (PI), and analyzed on LSR Fortessa (BD Biosciences).

To quantify mitochondria and lysosomes, or mitochondrial function, microglial cells were incubated with MitoTracker Green (Invitrogen, #M7514) and LysoTracker Green (Invitrogen, #L7526) in warm serumfree DMEM at 37  $^{\circ}$ C for 15 min. After incubation, ice-cold FACS buffer was added to terminate the reaction. Cell surface markers were labeled as described above. For reactive oxygen species (ROS) level detection, cells were incubated with CellRox Deep Red (Invitrogen, #C10422) in warm serum-free DMEM at 37  $^{\circ}$ C for 30 min. Cells were washed with ice-cold FACS buffer, followed by surface staining. The stained cells were resuspended in pre-chilled FACS buffer containing propidium iodide (PI) (Sigma-Aldrich, #P4864) and immediately analyzed with LSR Fortessa (BD Biosciences).

Microglia were first labeled with Zombie Aqua (BioLegend, #423102) and subsequently stained with surface fluorescence-conjugated antibodies mentioned above for the intracellular staining of proliferating cells and the mTOR pathway. The samples were fixed in the fixation buffer (Biolegend, #421401) and permeabilized with perm wash buffer (Biolegend, #421402). Cells were then incubated with p-mTOR (Ser2448) (eBiosciences, #12-9718-42) and p-4EBP-1(Thr36/Thr45) (eBiosciences, #12-9107-41). At the end of incubation, cells were washed and resuspended in FACS buffer and analyzed on the LSR Fortessa (BD Biosciences). Flow cytometry data were analyzed and graphed using FlowJo v10 (BD Life Sciences).

### 2.8. Immunofluorescence staining

For mouse brain tissue immunostaining, mice were anesthetized and transcardially perfused with 0.1 M PBS buffer and 4 % paraformaldehyde (PFA) (Merck, #1.04005.1000). The brains were removed and continuously post-fixed in 4 % PFA at 4 °C for 24 h, immersed in 30 % sucrose (Sigma-Aldrich, #9378) in 0.1 M PBS buffer for two days, and frozen with O.C.T. compound (Tissue-Tek®, #4583). Coronal brain serial sections, including cortex and striatum (approximately between bregma 0.86 and 0.14 mm) and hippocampus (approximately between bregma -1.34 and -2.3 mm), were cut using cryostats (Thermo Scientific, #NX70) and processed for immunostaining. Free-floating brain sections (20  $\mu m$ ) were permeabilized and blocked with 0.1 M PBS buffer containing 0.5 % Triton X-100 solution, 3 % BSA, and 7 % FBS for 2 h at room temperature. The brain sections were then incubated with the appropriate primary antibody in the blocking buffer at 4 °C overnight and then incubated with the corresponding secondary antibody at 4 °C for 4 h. The following primary and secondary antibodies were used in this study: rabbit anti-NeuN (Millipore, #ABN78), mouse anti-NeuN (Millipore, #MAB377), mouse anti-EM48 (Millipore, #MAB5374), rabbit anti-Iba-1 (Wako Laboratory Chemicals, #019-19741), goat anti-Galetin-3 (R&D System, #AF1197), rat anti-CD68 (Bio-Rad, #FA-11); Cy3-conjugated donkey anti-rabbit IgG (Jackson ImmunoResearch,

#711-166-152), Cv3-conjugated goat anti-rat IgG (Jackson ImmunoResearch, #112-165-167), Cy3-conjugated donkey anti mouse IgG (Jackson ImmunoResearch, #715-166-151), Alexa FluorTM 594 Goat anti-mouse IgG (Invitrogen, #A-11005), Alexa Fluor™ 647-conjugated donkey anti-rabbit IgG (Jackson ImmunoResearch, #711-606-152), Alexa Fluor<sup>TM</sup> 647-conjugated donkey anti-goat IgG (Jackson ImmunoResearch, #705-605-147). Nuclei were stained with 4',6-Diamidino-2-Phenylindole (DAPI) (Biolegend, #422801). Brain sections were attached to slides and mounted with the antifade mounting medium (Vector Laboratories, CA, USA). 20X magnification images were captured by AxioObserver 7 widefield microscope (Carl Zeiss, Germany) equipped with AxioCam 702 mono camera (Carl Zeiss, Germany) and were controlled by Zen 2.3 Blue software (Carl Zeiss, Germany). Three to five frames from one striatal section were analyzed and processed with Fiji ImageJ software (National Institutes of Health, USA) for the cell number quantitation or the intensity quantification. To observe the intracellular mHTT aggregates with higher resolution, 20X and 63X magnification of Z-stack images were captured by confocal microscopy (LSM700, Carl Zeiss, Germany).

The TUNEL assay was performed on  $10~\mu m$  thick brain sections using the Click-iT Plus TUNEL assay Alexa Fluor 647 kit (Invitrogen, #C10619). The sections were fixed with 4 % PFA, permeabilized using proteinase K for one hour at room temperature, and then subjected to washing steps. Terminal deoxynucleotidyl transferase (TdT) reaction was applied on sections to incorporate dUTP into the 3′ OH end of tissue sections and then incubated with TUNEL reaction mixture to label the incorporative dUTP with the fluorescent dye (Cy5). Negative (no TdT enzyme) controls were included in all experiments. The sections were washed with 0.1 M PBS buffer, stained with DAPI, and mounted with the antifade mounting medium. Tile images were obtained using an AxioObserver 7 widefield microscope (Carl Zeiss, Germany). The calculation of TUNEL+ cells in the striatum was done with IMARIS software (Version 8.0.2, Bitplane).

## 2.9. RNA preparation from human and mouse brain tissues, differential expressional level analysis, and quantitative real-time PCR

Total RNA extracted from HD and non-HD subjects' caudate nuclei and cerebellum were isolated using GENEzol<sup>TM</sup> TriRNA Pure Kit (Geneaid, #GZX100). cDNA was synthesized using SuperScript<sup>TM</sup> III Reverse Transcriptase (Thermofisher, #18080093). Quantitative realtime PCR using the  $2^{-\Delta \Delta CT}$  method determined the relative mRNA level. 18S ribosomal RNA was used as the reference genes for the mouse and human postmortem brain samples. The primers used in this study are listed in Supplemental Table 1. Human postmortem tissue (caudate nuclei and cerebellum) used for qPCR analysis was obtained from the Human Brain and Spinal Fluid Resource Center (VA West Los Angeles Healthcare Center, Los Angeles, CA, USA). Each subject's demographic and neuropathological information are listed in Supplemental Table 2. Total RNA from mouse striatum or cerebellum was extracted using TRI reagent (Invitrogen, #AM9738) according to the manufacturer's protocol. Reverse transcription was performed as described above and qPCR was performed on StepOnePlusTM Real-Time PCR System (Applied Biosystems) using 2X TaqMan Universal Master Mix II with UNG (Applied Biosystems, #4440038) and TaqMan probes, Slc29a3 (Mm00469913 m1). The gene expression level was normalized to the reference gene, Rpl19 (Mm02601633\_g1), and calculated as relative quantification.

The relative transcript level (differential expression, DE) of the ENT3 gene (SLC29A3) in the postmortem prefrontal cortex of 157 non-HD subjects and 127 HD patients was derived from gene expression data collected in a previous study (Narayanan et al., 2014). The expression data was adjusted for the same covariates (such as age and gender) as in the earlier study using the same method, robust linear regression (rlm), except for one difference: Instead of fitting an rlm model of each gene expression data separately for the HD and control groups using the

covariates as in the previous study, we fit an rlm model of each gene expression data once using all HD and control expression values to ensure that the DE signal is not lost in the adjustment.

### 2.10. Cytokine production profile of microglia

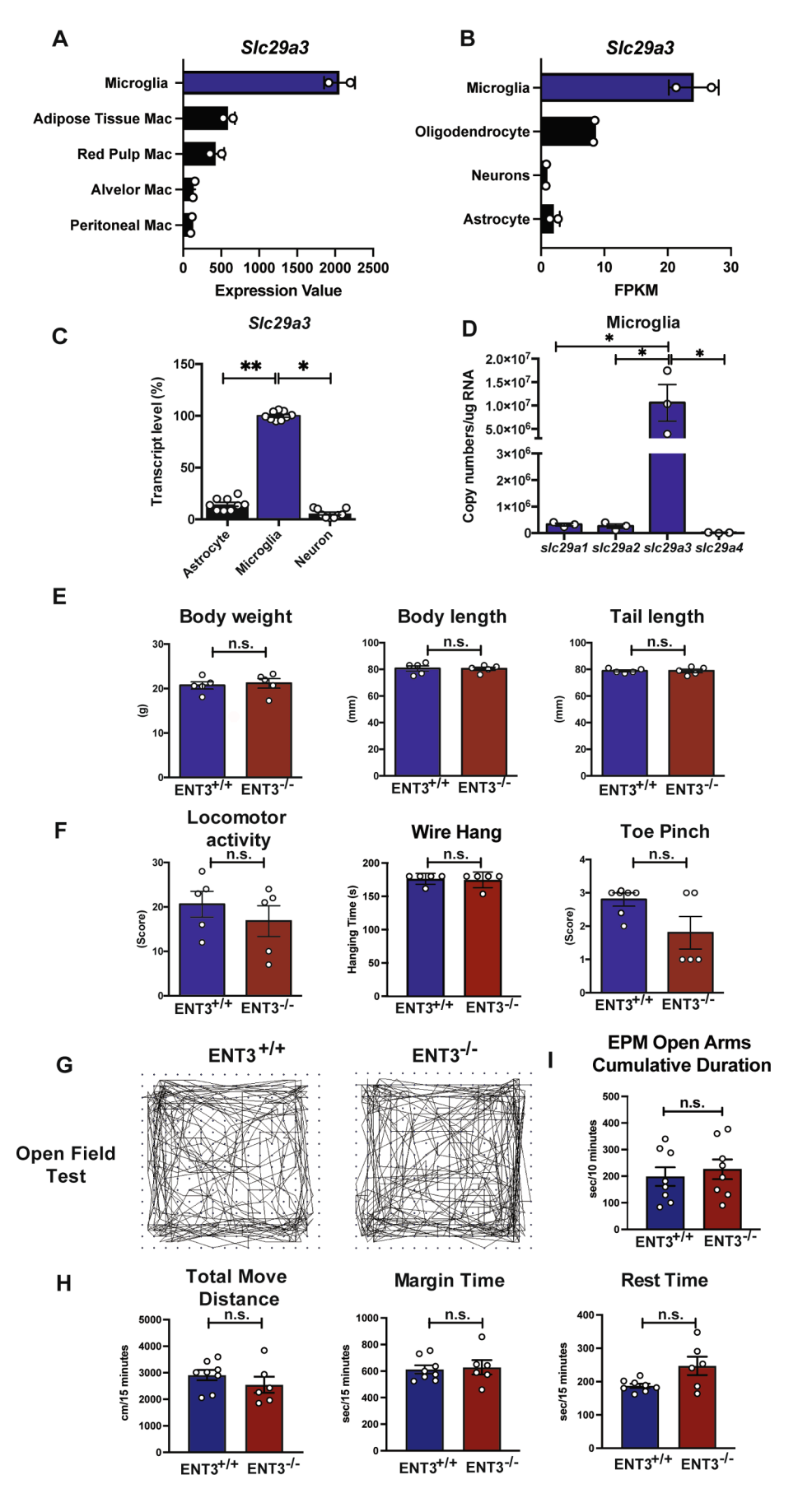
Microglia were prepared from 12-week-old adult mice brains, and the total RNA was extracted using TRI reagent (Invitrogen, #AM9738) according to the manufacturer's protocol. Reverse transcription was performed by using SuperScript III Reverse Transcriptase (Invitrogen, #18080051) with oligo (dT) 20 (Invitrogen, #18418020), dNTP mix (Invitrogen, #18427-013), and RNaseOUT (Invitrogen, #10777019). qPCR was performed on StepOnePlusTM Real-Time PCR System (Applied Biosystems) using 2X TaqMan Universal Master Mix II with UNG (Applied Biosystems, #4440038) and TaqMan probes. The gene expression level was normalized to the reference gene, Rpl19 (Mm02601633 g1), and calculated as relative quantification. The following TaqMan probes ordered from Invitrogen were used in this study: Tnf (Mm00443258 m1), (Mm00434228 m1), 116 (Mm00446190 m1). (Mm00475988 m1), Il10 (Mm01288386 m1).

#### 2.11. Clasping and rotarod tests

The body weight of the mice was measured and documented three times per week, starting from 7 weeks of age until 13 weeks. The limbclasping behavior test in mice involved suspending the mice (at the age of 7–13 weeks) by their tails for 30 s. Scoring was based on the following criteria: a score of 0 indicates no clasping when no limb retracts to the abdomen, a score of 1 is given when either the forelimbs or hind limbs retract, and a score of 2 is assigned when both the forelimbs and hind limbs retract. Each testing session consisted of a single trial. The average score for each week was calculated based on the results obtained from these trials. Motor coordination was assessed using a rotarod apparatus assay (Life Science, ROTO-ROD Series 8). Briefly, the mice were tested three days per week from 7 to 13 weeks, with three trials conducted each day. Each trial had a maximum duration of 120 s, and the speed was kept constant at 12 rpm. The most prolonged latency to fall observed on the same day represented the daily score. The average of the longest time obtained from three days represented the score for the week.

## 2.12. Filter retardation assay and western blotting

Filter retardation assay (FRA) was performed to quantify the SDSinsoluble mHTT aggregates in the mice striatal lysates as previously described (Lee et al., 2022). The striatal homogenate was prepared in PBS with 2 % SDS and then applied onto a slot blot manifold (Bio-Rad, Hercules, CA, USA) with a cellulose acetate membrane (0.2 µm pore size). The membrane was blocked with 5 % skim milk and incubated overnight at 4 °C with Habe1 (Chern's lab-generated anti-HTT antibody), followed by incubation at room temperature with goat antimouse-HRP (1:10000, Jackson ImmunoResearch, #115035166). Striatal tissue was prepared in RIPA lysis buffer (150 mM NaCl, 50 mM Tris-HCl pH 8, 1 % Triton-100, 0.5 % sodium deoxycholate, and 0.1 % SDS) containing protease inhibitor cocktail (Calbiochem, #539131-10VL) and phosphatase inhibitor (PhosSTOP<sup>TM</sup>) (Roche, #4906845001). The resulting samples were electrophoresed by 10 % SDS-PAGE. Proteins were then transferred to PVDF membranes, blocked, and then incubated at 4 °C overnight with rabbit anti-mouse PINK1 (Novus Biologicals, BC100-494), mouse anti-mouse Parkin (Cell signaling, #4211), rabbit anti-mouse GAPDH (GeneTex, GTX100118), or mouse anti- $\beta$ -actin antibody (Sigma, #A5441), followed by the goat anti-rabbit (GeneTex, GTX213110-041) or goat anti-mouse IgG-HRP (Jackson ImmunoResearch, #115035166) were used as the control. The immunoblots were developed with SuperSignal<sup>TM</sup> West Pico PLUS Chemiluminescent substrate (Thermo Scientific™, #34577), and signals were detected by LAS-4000 (Fujifilm) and were quantified using ImageJ.



(caption on next page)

Fig. 1. ENT3 is highly expressed in microglia, but the deficiency of ENT3 does not generate gross physical and behavioral defects in the mice. (A) RNA-Seq data of selected tissue-resident macrophages were extracted from the ImmGen database (http://www.immgen.org). The expression value of slc29a3 was normalized by DESeq2, N = 2. (B) The expression profile of ENT3 in major types of brain cells was evaluated by mining the Brain RNA-Seq database (www.BrainRNAseq.org), N = 2. (C) Relative expression levels of slc29a3 in primary adult astrocytes, microglia, and neurons were evaluated by qPCR. The expression vector of slc29a3 was used to develop a standard curve to calculate the absolute copy number and expressed as transcript levels. (N = 9). (D) Absolute quantification of slc29a1, slc29a2, slc29a3, and slc29a4 in isolated adult microglia was determined by qPCR. The expression vectors of each slc29 family member were applied to generate standard curves for calculating the absolute copy number (N = 3). One-way ANOVA followed by Turkey's multiple comparisons test was applied. \*p < 0.05, \*p < 0.005. (E) The modified SHIRPA test was performed to examine the gross physical appearance. (F) Locomotor activity, wire hang, and toe pinch tests were performed to evaluate the motor function of ENT3<sup>-/-</sup> and WT littermates (N = 5). (G) Representative movement-tracking results of ENT3<sup>-/-</sup> and littermate in open field test. (H) The quantification of total move distance, margin time, and rest time of ENT3<sup>-/-</sup> and littermate under open field test (N = 6–8). (I) Elevated plus maze test was performed on ENT3<sup>-/-</sup> and littermate; the cumulative duration in the open arm was shown (N = 8). Statistical analyses were performed with unpaired t-tests, n.s., not significant. All results were presented as mean  $\pm$  SEM.

### 2.13. Primary microglial degradation assay

Adult microglia were harvested from 12-week-old mouse brains. The purified microglia were seeded in a poly-D-Lysine coated glass-bottom dish containing complete DMEM and incubated at 37C with 5 %  $\rm CO_2$  for 48 h before the experiment. To obtain apoptotic cells, the thymocytes of ROSA26 mice were treated with 10  $\mu M$  dexamethasone (Sigma-Aldrich, D4902) in complete DMEM for 6.5 h. The resulting apoptotic thymocytes were added to the microglia culture at a 10:1 ratio for 2 h. At the end of the incubation, the non-phagocytosed cells were removed by rinsing the culture with PBS. Fresh medium was replaced and returned to culture for an additional 14 hr before being subject to immunofluorescent microscopic observation. The degree of apoptotic cell degradation was evaluated by the presence of GFP signals within microglia.

#### 2.14. Ex vivo brain metabolic assessment

Metabolic assessment of live brain slices was evaluated using the Seahorse XFe24 system (Agilent Technologies) based on the protocol described (Qi et al., 2021). Briefly, mice were decapitated, and the brain was rapidly removed and immersed in ice-cold artificial cerebrospinal fluid (aCSF) (containing 120 mM NaCl, 3.5 mM KCl, 1.3 mM CaCl<sub>2</sub>, 1 mM MgCl<sub>2</sub> hexahydrate, 0.4 mM KH<sub>2</sub>PO<sub>4</sub>, and 5 mM HEPES supplemented with 4 g/L BSA and 10 mM sucrose). The 250 µm coronal brain slices (+0.86 to +0.26 mm from bregma (Hong et al., 2012)) were prepared in aCSF using a vibratome (Leica VT 1000S). The circular striatal slices were obtained from the middle to lateral dorsal striatum of the coronal brain slices by 1-mm stainless steel biopsy punchers. They were transferred into the XFe24 Islet Capture Microplate. The circular striatal slices were incubated with aCSF at 37 °C in a CO2-free incubator for 1 h, and the Seahorse assay was further performed. The baseline of Oxygen Consumption Rate (OCR) and Extracellular Acidification Rate (ECAR) were measured, and sequential injections of 25 μM oligomycin A (Sigma-Aldrich, #O4876), 10 µM FCCP (Sigma-Aldrich, #C2920), and 20 μM Antimycin A (Sigma-Aldrich, #A8674) were applied for respiratory capacity measurements. The parameters were recorded three times after each drug injection. The results were analyzed using the Seahorse Wave Desktop Software (Agilent Technologies).

## 2.15. Software and statistical analysis

All statistical analyses and graphing were done with Prism 6.0 (GraphPad). The results were presented as the mean  $\pm$  SEM, and they were analyzed by unpaired two-tailed Student's t-tests, one-way or two-way analysis of variance (ANOVA), followed by pairwise comparisons using Tukey's or Fisher's LSD test. Survival was evaluated by the log-rank (Mantel-Cox) test. P values < 0.05 were considered statistically significant.

## 3. Results

3.1. Slc29a3 is highly expressed in microglia, but its deficiency does not impact the general physical characteristics and behaviors of the cells

Previously, we have compared the expression of slc29a3 in different immune cell populations (Hsu et al., 2012). Knowing that it is highly expressed in myeloid-lineage cells, we extracted RNAseq results from the ImmGen database (https://www.immgen.org). We found that the brain resident macrophages, microglia, have the highest expression level of slc29a3 among all tissue-resident macrophages (Fig. 1A). Across the major brain cell populations, microglia have a significantly higher expression of slc29a3 than oligodendrocytes, neurons, or astrocytes by RNAseq or qPCR analyses (Fig. 1B and C). When comparing the copy number of different slc29 family member transcripts, it is clear that slc29a3 is the dominant nucleoside transporter expressed in microglia (Fig. 1D). With such a high level of expression in the microglia, we deliberated whether the deletion of ENT3 may impact the general physical or locomotive capacity in mice. The modified SmithKline, Harwell, Imperial College, Royal Hospital, Phenotype Assessment (SHIRPA), and wire hang test were performed on 10- to 12-week-old ENT3<sup>-/-</sup> and littermate mice (Fig. 1E and F) to evaluate the mice's motor activity, coordination, postural control, muscle tone, autonomic functions, and emotional reactivity, as well as any reflexes dependent on visual, auditory, and tactile modalities. No apparent physical differences were found comparing the ENT3<sup>-/-</sup> to their littermates. We then performed the open field test (Fig. 1G and H) and elevated plus maze test (Fig. 1I) to monitor their moving ability and the mice's level of anxiety, and no statistically significant differences were noted in the parameters examined between WT littermates and ENT3<sup>-/-</sup> mice. These results suggest that although ENT3 is highly expressed in microglia, the deficiency of ENT3 does not result in a general neurological defect under a homeostatic state.

## 3.2. ${\it ENT3^{-/-}}$ brain showed microglial hyperplasia without active inflammation

The peculiar high expression level of slc29a3 in microglia and the prior observation of myeloid-proliferative phenotype in the peripheral tissue of ENT3<sup>-/-</sup> mice (Hsu et al., 2012) prompted us to perform a detailed analysis of microglia. Adult mice microglia were harvested from brain tissue through enzyme digestion and Percoll gradient separation. The resulting microglial-enriched fraction was subjected to flow cytometric analyses. Defined as CD11b+CD45low population (Fig. 2A), we found that although ENT3-/- mice had slightly lower percentage of microglia in the fraction (Fig. 2B), the number of microglia was significantly increased (Fig. 2C). These microglia were further examined for multiple surface markers including MHCII for antigen presentation, CD80 and CD86 for activation, CD206 for M2-like phenotype, and TIM4 for phagocytic receptor expression. We found no differences in the expression of these markers between ENT3<sup>-/-</sup> and littermate microglia (Fig. 2D and E), implying a lack of alteration of general phagocytic cell phenotypes on  $\mathrm{ENT3}^{-/-}$  microglia. Although flow cytometric analysis

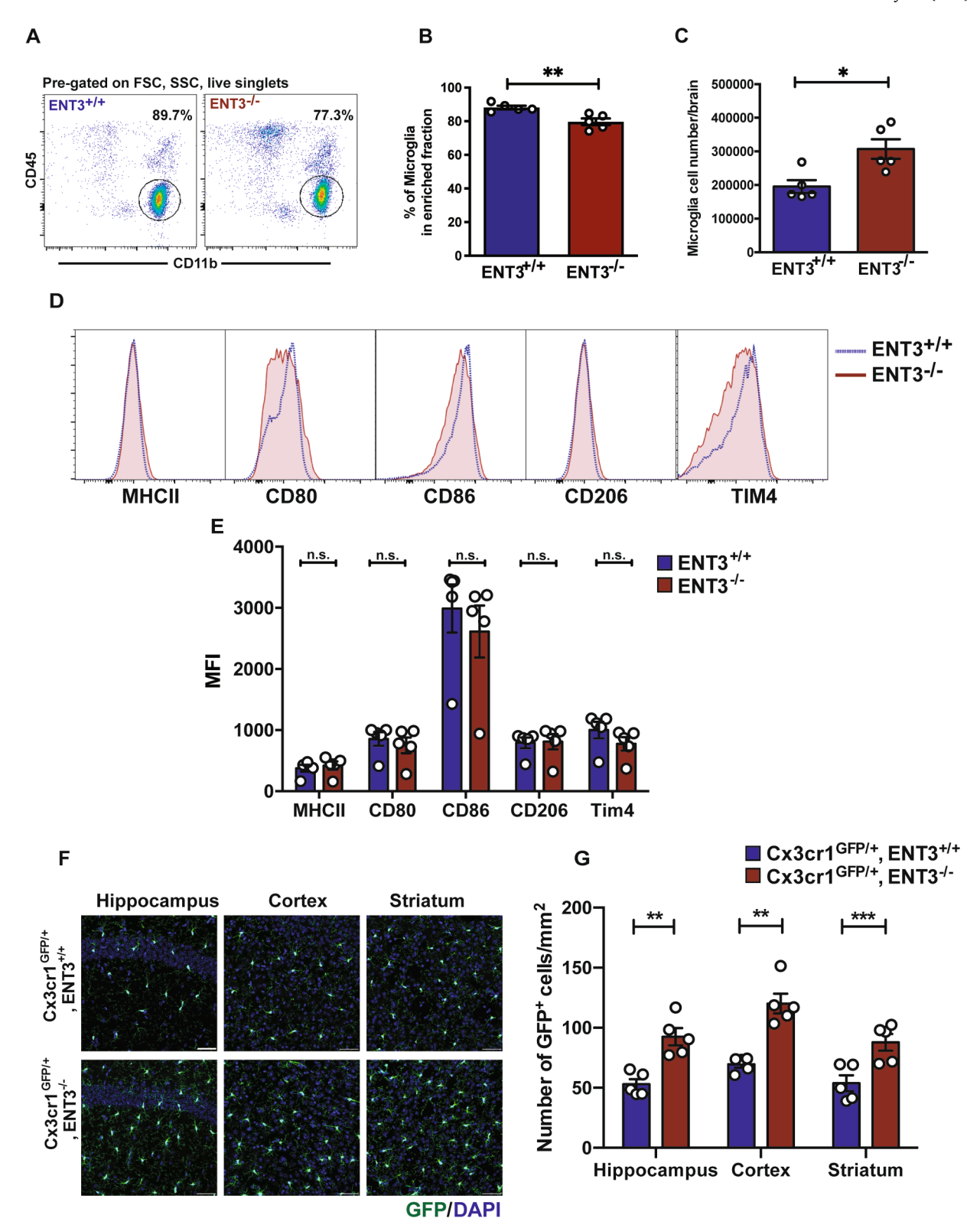


Fig. 2. ENT3 deficiency leads to microglial hyperplasia without altering their surface phenotypes. (A) Primary adult microglia were harvested by enzyme digestion followed by Percoll enrichment and subjected to flow cytometric analysis. The representative results illustrated that the microglia population was defined as live singlets expressing CD11b+CD45<sup>low</sup> population. The percentage (B) and absolute number (C) of microglia in the enriched preparation of the adult brain were shown (N = 5). (D) Multiple surface marker expressions of ENT3<sup>-/-</sup> and littermate microglia were evaluated by flow cytometric analyses, and (E) quantified by the mean fluorescent intensity (MFI) (N = 5). (F) The ENT3<sup>-/-</sup> mice were crossed with Cx3cr1<sup>GFP/+</sup> mice to perform *in vivo* lineage tracing for microglia. The brain sections of the hippocampus, cortex, and striatum were visualized using a fluorescent microscope. Scale bars = 50  $\mu$ m. (G) The quantification of GFP<sup>+</sup> microglia in each brain area. Ten fields were taken for every section; three sections were collected and quantified per mouse (N = 5). All results were presented as mean  $\pm$  SEM. Statistical analyses were performed with unpaired *t*-tests. \*p < 0.05, \*\*p < 0.01, \*\*\*p < 0.001, n.s., not significant.

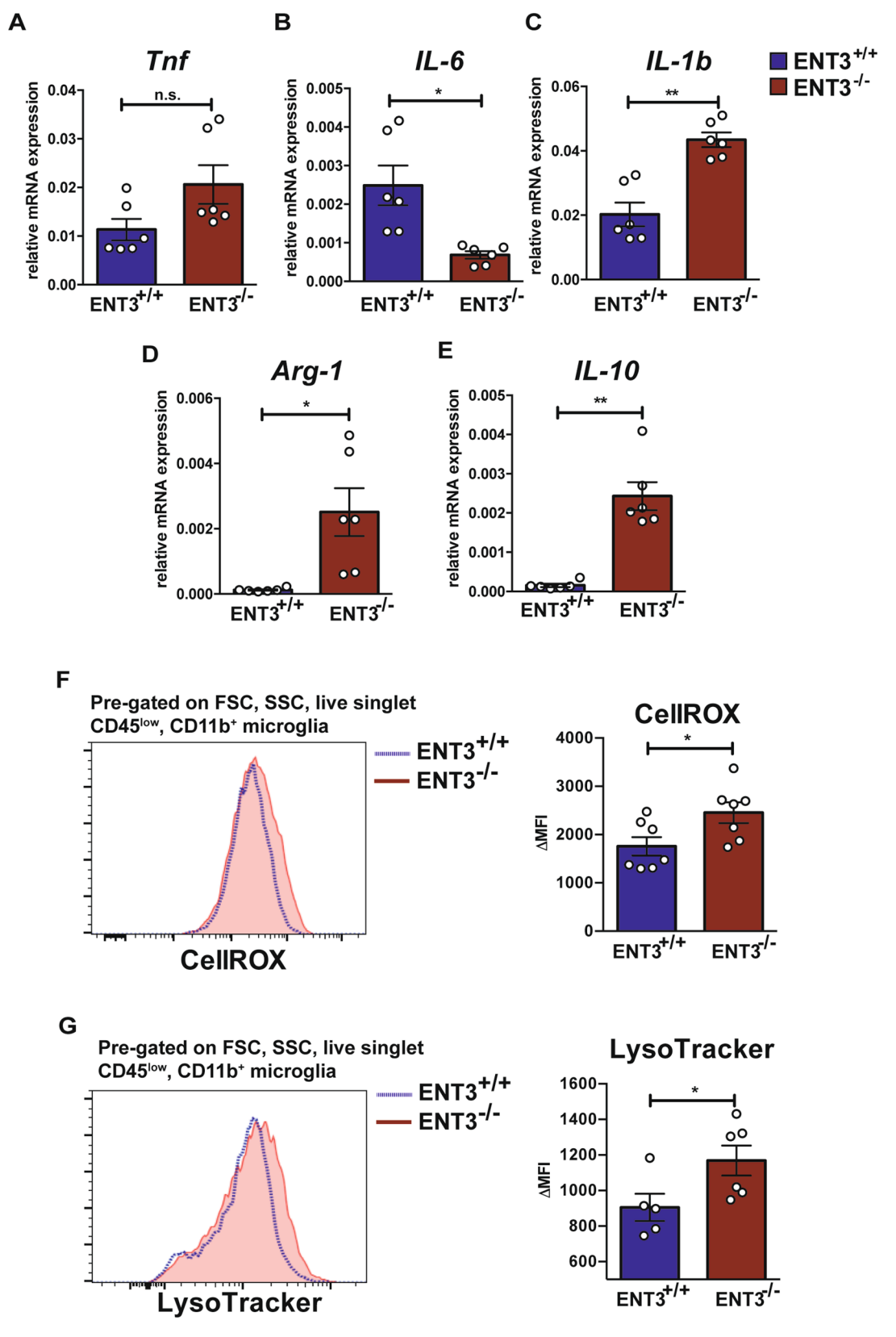


Fig. 3. ENT3 $^{-/-}$  microglia have increased production of cytokines, harbor elevated levels of cellular ROS, and possess larger lysosomal compartments. The primary adult microglia were enriched, purified via CD11b magnetic microbeads, and subjected to qPCR analysis. The relative mRNA expression levels of proinflammatory cytokines Tnf (A), IL-6 (B), IL-1 $\beta$  (C), and anti-inflammatory effectors Arg-1 (D) and IL-10 (E) in the microglia were measured (N = 6). (F) Cellular ROS level was evaluated by subjecting the microglia to CellROX staining and analyzed by flow cytometry (N = 7). (G)The microglial lysosomal compartment was measured by LysoTracker staining (N = 5-6). The  $\Delta$ MFI was calculated by total MFI minus the fluorescence minus one (FMO) background value. All results were presented as mean  $\pm$  SEM. Statistical analyses were performed with unpaired t-tests. \*p < 0.05, \*\*p < 0.01, n.s., not significant.

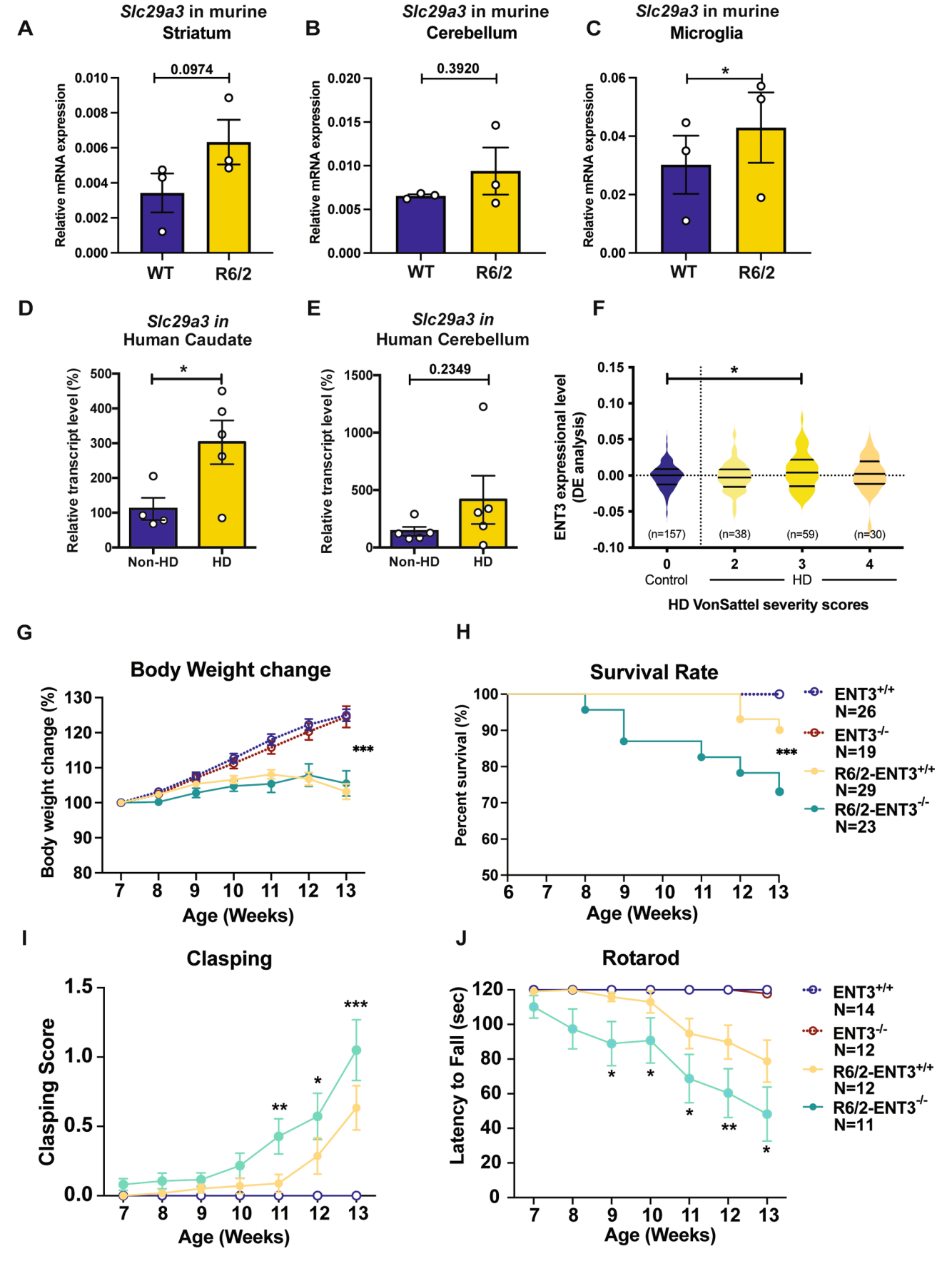


Fig. 4. The increased expression of ENT3 is observed in both the R6/2 HD mouse model and human HD patients, and the deficiency of ENT3 worsens the HD-like phenotype in R6/2 mice. Mouse (A) striatum and (B) cerebellum were harvested from R6/2 and WT littermate. The expression level of the slc29a3 transcript was evaluated by qPCR analyses. (C) The Primary adult microglia were harvested from R6/2 and littermate brain tissues and subjected to qPCR analysis. The expression of slc29a3 was normalized to the reference gene, Rpl19, and expressed as relative expression levels (N = 3). Paired t-test was applied, \*p < 0.05, or labeled on the graphs. The expression of ENT3 in the postmortem human caudate nucleus (N = 4-5) (D) and cerebellum (N = 5) (E) from non-HD and HD patients was evaluated by qPCR analyses. (F) The differential expression (DE) levels of ENT3 expression in the postmortem prefrontal cortex from non-HD and HD patients were analyzed and shown in the violin plot. Disease severity was determined using Vonsattel severity scores. The subject number of each grade was indicated on the graph. The expression level of ENT3 at score 0 was used as a control. All values were shown as mean  $\pm$  SEM. Statistical analyses were performed with unpaired t-tests. \*p < 0.05 or labeled on the graphs. (G) The body weight change of the mice was monitored throughout the behavior test and showed in percentages (%). Two-way ANOVA with Tukey's multiple comparisons was applied, and significant differences between WT and R6/2 mice were labeled with asterisks, \*\*p < 0.001. (H) The survival curve during the study period. (I) The clasping behavior of the mice was scored. (J) The latency of falling from the rotarod was documented. Two-way ANOVA with Tukey's multiple comparisons was applied. Statistically significant differences between R6/2 ENT3<sup>+/+</sup> and R6/2 ENT3<sup>-/-</sup> in (H, I, J) were labeled with asterisks, \*p < 0.005, \*p < 0.005, \*p < 0.005, \*p < 0.005.

provides abundant information regarding the surface phenotype, it lacks spatial detail. To clearly identify if the microglial hyperplasia is limited to a specific brain area, we crossed the microglia-tracing Cx3cr1-GFP to ENT3<sup>-/-</sup> and observed a consistent increase of microglia in the hippocampus, cortex, and striatum in the Cx3cr1<sup>GFP/+</sup>ENT3<sup>-/-</sup> brain (Fig. 2F and G). These results together demonstrated that in the absence of ENT3, the brain tissue has an increased number of microglia, but unlike in typical microgliosis, no elevation of surface activation markers was noted on the ENT3<sup>-/-</sup> microglia. This data is consistent with the histiocytosis phenotype or intestine of ENT3<sup>-/-</sup> mice (Hsu et al., 2012) and skin biopsies of patients carrying ENT3 mutations (Bloom et al., 2017).

# 3.3. The ENT3<sup>-/-</sup> microglia are M2-prone and harbor higher reactive oxygen species (ROS) stress together with a larger lysosomal compartment

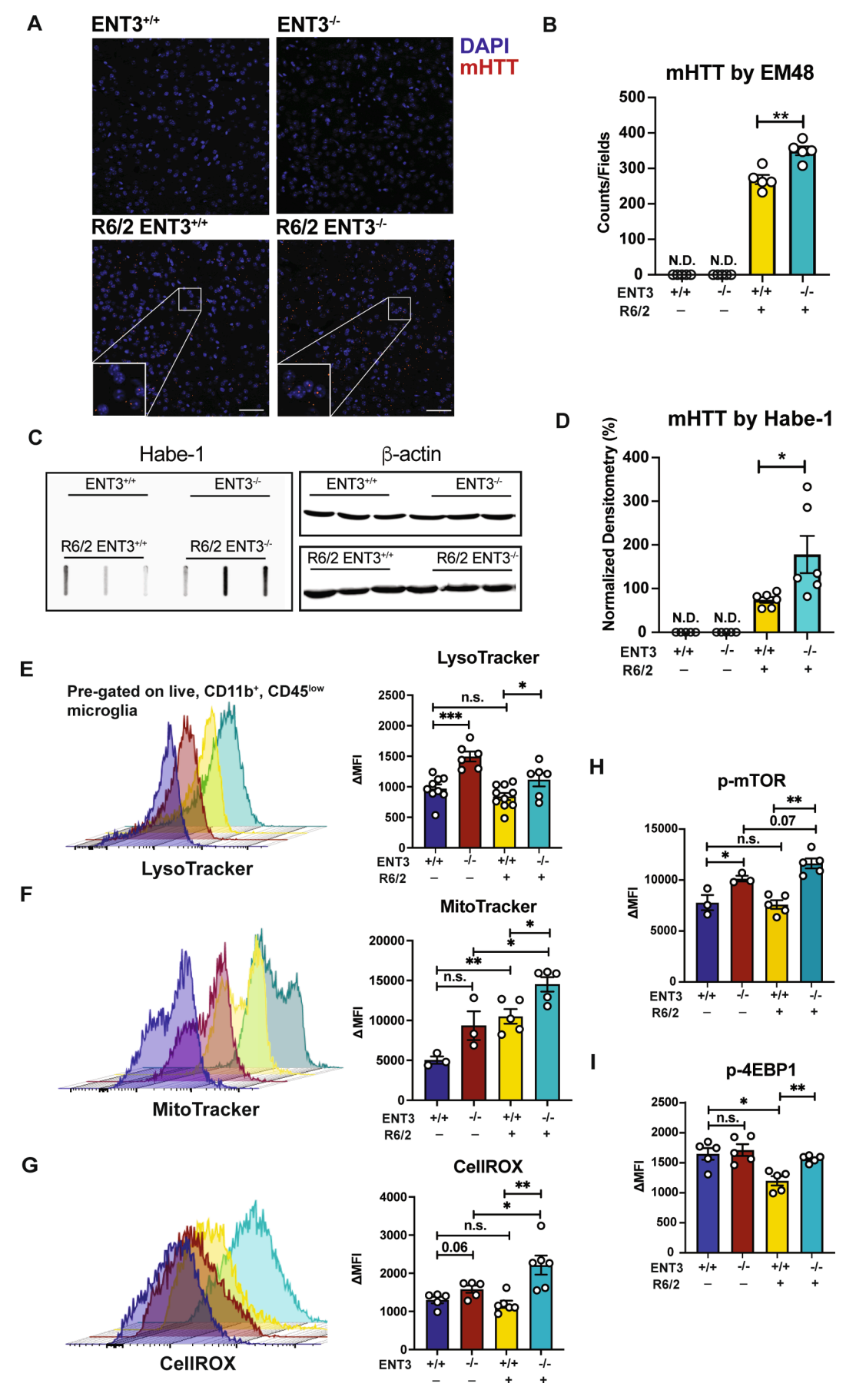
Although no significant changes on the typical macrophage surface markers were noted between ENT3<sup>-/-</sup> and littermate microglia, we wondered if they have functional differences. The primary adult microglia were purified and evaluated for their cytokine production profiles and cellular stresses. By qPCR analyses, we found that ENT3<sup>-/</sup> microglia have significantly higher transcription of *IL-1β*, *Arg-1*, and *IL-*10, but not Tnf and IL-6 compared to WT cells (Fig. 3A-E). This cytokine expression profile and the surface marker pattern confirm that ENT3<sup>-/</sup> microglia are not under the typical proinflammatory polarization status. Instead, they are more prone to the reparative M2 phenotype. While these ENT3<sup>-/-</sup> microglia were actively transcribing the immunosuppressive IL-10 and Arg-1, they experienced higher cellular ROS stress (Fig. 3F) and harbored larger lysosomal compartments (Fig. 3G). The alteration of the lysosomal compartment has been observed prior in ENT3-deficient splenic macrophages (Hsu et al., 2012), suggesting that it is a shared defect in ENT3<sup>-/-</sup> tissue-resident macrophages and likely a reflection of dysfunctional lysosomes in the ENT3<sup>-/-</sup> microglia.

## 3.4. Elevated ENT3 expression in the brain plays a protective role in Huntington's disease

As a progressive neurodegenerative disease, HD is characterized by the accumulation of mHTT and reactive microglia (Sapp et al., 2001). Two subcellular pathways are known to be responsible for the clearance of mHTT - the ubiquitin-proteasome system (UPS) and autophagy (Zhao et al., 2016). Considering the high expression level of ENT3 in microglia and its involvement in lysosome-mediated activities, we speculated that ENT3 may have a role in the pathogenesis of HD. Primary brain tissue and adult microglia were harvested from WT and the HD mouse model, R6/2 mice, and subjected to slc29a3 expression analysis. We found that the striatum and cerebellum tissue of R6/2 mice appeared to show a trend of increased slc29a3 expression (Fig. 4A and B). At the same time, their microglia had significantly upregulated the expression of slc29a3 (Fig. 4C), alluding to an association between ENT3 and HD. Quantitative PCR analyses of HD patients' caudate and cerebellum were performed, confirming the consistently higher expression level of slc29a3 in HD patients compared to non-HD subjects (Fig. 4D and E). When comparing the microarray results (Narayanan et al., 2014) from human postmortem prefrontal cortex tissue from non-HD and HD subjects, we noted a positive correlation between disease severity and the expression of slc29a3 (Fig. 4F). These observations together strongly implied the potential involvement of ENT3 in HD progression. The upregulation of ENT3 expression in both human HD patients and the R6/2 disease model may be explained by two scenarios – ENT3 may have acted as a compensatory response to protect the brain from further damage or as one of the causes leading to pathogenesis. To delineate these two possibilities, we generated an R6/2 ENT3<sup>-/-</sup> mouse strain and studied the disease progression in these mice. While we did not observe body weight differences between the ENT3<sup>+/+</sup> and ENT3<sup>-/-</sup> genotypes, the mice in the R6/2 background showed significantly lower weight at 13 weeks of age (Fig. 4G), while the R6/2 ENT3<sup>-/-</sup> had a higher fatality rate than all control groups (Fig. 4H). Notably, the fatality of male R6/2 ENT3<sup>-/-</sup> mice started as early as eight weeks old, and only 50 % of the population survived until 13 weeks old (Supplemental Fig. 1). Due to this complication, we used female R6/2 ENT3<sup>-/-</sup> to perform motor function tests. The motor function evaluations showed that  $R6/2\ ENT3^{-/-}$  had a significantly higher clasping score (Fig. 4I) and inferior rotarod performance (Fig. 4J) compared to R6/2 littermates starting at nine weeks of age, while no abnormalities or differences were noted between ENT3<sup>+/</sup> and ENT3<sup>-/-</sup>. These results suggested that the absence of ENT3 worsens the HD-like disease progression in R6/2 mice, and ENT3 has a protective role during the pathogenesis of HD in the R6/2 disease model.

## 3.5. Accumulation of mHTT and the disturbed microglial homeostasis in $R6/2\ ENT3^{-/-}$ mice

Since the accumulation of mHTT is a hallmark contributor to HD patients' loss of motor control, we performed immunofluorescence staining (IF) to evaluate the degree of striatal mHTT deposition. We found a significantly higher amount of mHTT was observed in the R6/2 ENT3<sup>-/-</sup> striatal section compared to R6/2 littermates (Fig. 5A and B). This observation was further confirmed via filter retardation assay (FRA) on striatal tissues (Fig. 5C and D). Both IF and FRA results showed that the absence of ENT3 leads to increased mHTT accumulation in the striatum. The results from motor function evaluations (Fig. 4I and J) and mHTT quantification analyses together imply that ENT3 may facilitate the degradation of mHTT during HD pathogenesis. Since ENT3 has been associated with lysosomal-mediated activities (Hsu et al., 2012) (Wei et al., 2018), we speculate that the phenotypes observed in R6/2 ENT3<sup>-/</sup> may be a result of microglial disturbances. We found that R6/2  ${
m ENT3^{-/-}}$  microglia had significantly enlarged lysosomal compartments compared to R6/2 littermates (Fig. 5E). Lysosomes are not only responsible for the degradation of cell debris or misfolded proteins but also for the removal of aged or damaged organelles via autophagy. Accordingly, we observed that the R6/2 ENT3<sup>-/-</sup> microglia had a significant accumulation of mitochondria (Fig. 5F) and were under elevated cellular ROS stress (Fig. 5G). These results can be explained as either defective mitophagy or as a compensatory measure for energy generation. As lysosomes and mitochondria are both integral



(caption on next page)

Fig. 5. Accumulation of mHTT and the disturbed microglial homeostasis are observed in R6/2 ENT3 $^{-/}$ . (A) The presence of mHTT aggregates in the striatum area was evaluated by immunofluorescent staining with the anti-mHTT (EM48) antibody. Scale bars = 20 µm. (B) mHTT accumulation was quantified by enumerating the EM48 signal in each field. Six fields were taken for every section; three sections were collected and quantified per mouse (N = 5). (C) anti-mHTT (Habe-1) antibody was applied in filter retardation assay to evaluate the amount of mHTT in the brain. (D) The Habe-1 signal was quantified by normalization to the loading control,  $\beta$ -actin (N = 6). N.D., not detected. Primary microglia were harvested and enriched for their cellular status evaluations. (E) The microglial lysosome volume was monitored by LysoTracker staining (N = 6–10). (F) The number of mitochondria in microglia was measured by MitoTracker labeling (N = 3–5). (G) The cellular ROS was evaluated by CellRox staining (N = 5–6). The activation of the mTOR pathway in microglia was examined by microglial intracellular staining of p-mTOR (H) and p-4EBP-1 (I), followed by flow cytometric analysis (N = 3–5). All values were shown as mean  $\pm$  SEM. Statistical analyses were performed with unpaired t-tests. \*p < 0.05, \*\*p < 0.001, \*\*\*p < 0.001, n.s., not significant.

components of the energy production machinery in the cell, we examined the activity of mTOR, a key regulator of cellular metabolism. We found that R6/2 ENT3<sup>-/-</sup> microglia showed increased levels of p-mTOR (Fig. 5H) and p-4EBP1 (Fig. 5I) compared to R6/2 littermates. These results suggest that ENT3 has a vital role in clearing mHTT and maintaining microglial homeostasis.

### 3.6. ENT3 ameliorates HD-induced microglial stress

The disturbed microglial homeostasis phenotypes in the R6/2 ENT3<sup>-/-</sup> mice prompted us to hypothesize that these microglia may be dysfunctional. To test this possibility, we examined the lysosomal membrane integrity using galectin-3 (Gal-3) staining (Aits et al., 2015). We observed a prominent cluster of Gal-3<sup>+</sup> microglia in R6/2 ENT3<sup>-/-</sup> striatum (Fig. 6A), indicating a disruption of lysosomal integrity in these cells. Quantification of the IF results showed a significant increase in Gal-3 signals under HD stress, which was further exacerbated in the absence of ENT3 (Fig. 6B). A similar pattern was noted in Iba-1 signals (Fig. 6C), further highlighting the connection between ENT3 deficiency and disturbance in microglia homeostasis. These results suggest that ENT3 is crucial in supporting microglial lysosomal integrity and function, particularly under HD-like stress conditions. To investigate the physiological consequences of ENT3 deficiency in the HD setting, we stained the striatal section to explore the relationship between R6/2 ENT3<sup>-/-</sup> microglia functional alteration and mHTT accumulation. CD68/Macrosialin, which belongs to the family of LAMP proteins located in the lysosomal membrane, was applied to evaluate the lysosomal compartment (Chistiakov et al., 2017). We found that while mHTT aggregates were presented as small puncta that were evenly distributed in R6/2 ENT3<sup>+/+</sup>, the mHTT appeared to be in much larger aggregates within R6/2 ENT3<sup>-/-</sup> microglia, which were significantly bigger with higher CD68 signals (Fig. 6D and Supplemental Fig. 2). This observation suggested that the R6/2 ENT3<sup>-/-</sup> microglia may have defects in their processing of engulfed materials. To test this possibility, we set up an ex vivo system co-culturing the primary microglia with apoptotic cells to evaluate the degradational capacity of microglia (Fig. 6E). We found that R6/2 ENT3 $^{-/-}$  microglia harbored a significant accumulation of un-degraded apoptotic cells compared to the control group (Fig. 6F). This data collectively demonstrates that ENT3 deficiency has a clear impact on the R6/2 microglia, leading to the loss of lysosomal membrane integrity and accumulation of undigested mHTT or apoptotic cells, highlighting the indispensable support ENT3 provides to microglia, which are protective to HD progression.

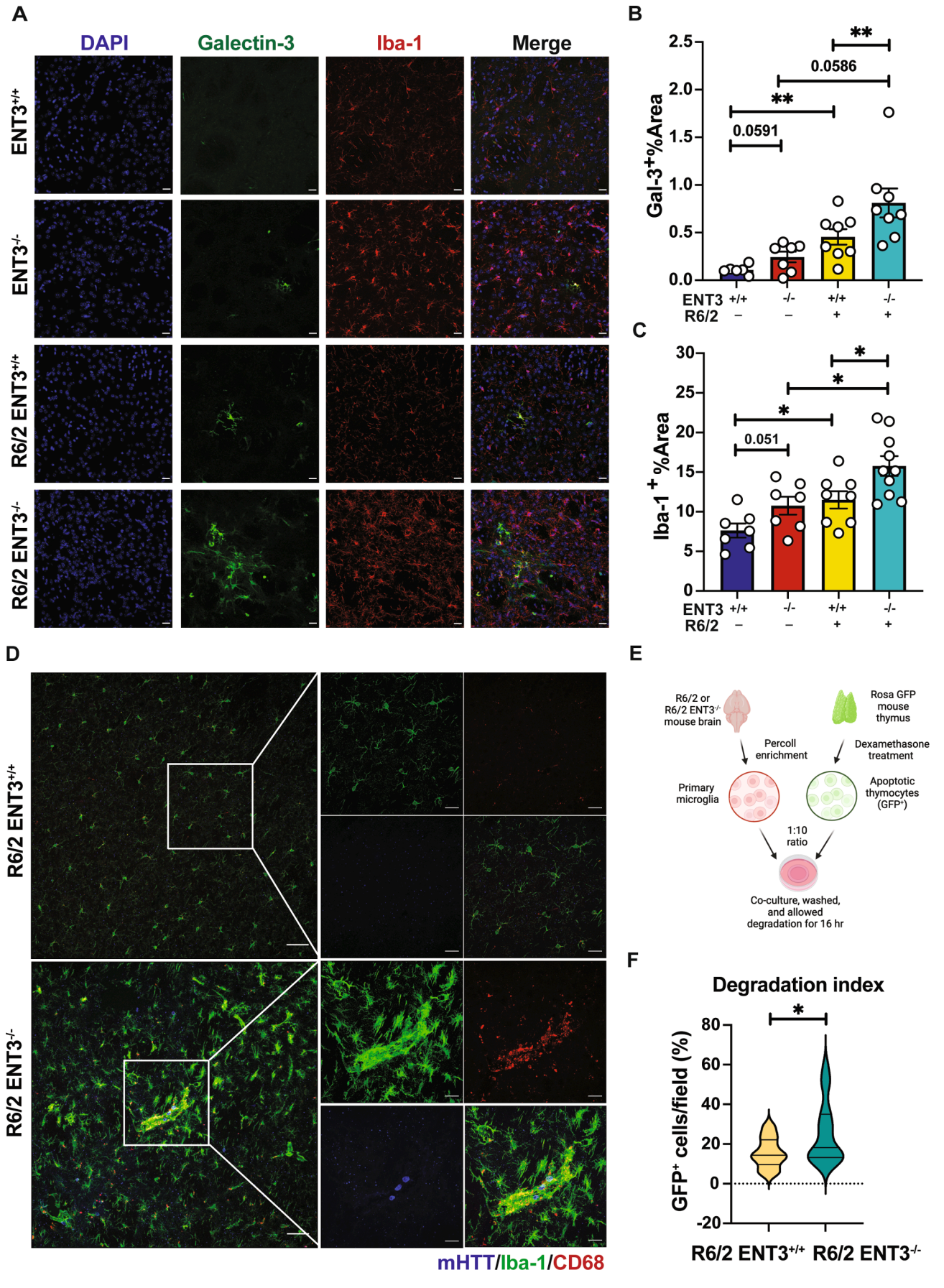
## 3.7. Deficiency of ENT3 results in the energy crisis in HD-like R6/2 mouse brain

Having observed the microglial abnormalities in the absence of ENT3, we wondered about ENT3 absence's overall impact on the brain striatum. We found that NeuN<sup>+</sup> cells were significantly rarer in R6/2 mice, a hallmark feature of mature neuron degeneration, and a further decrease of NeuN<sup>+</sup> cells was noted in R6/2 ENT3<sup>-/-</sup> striatum (Fig. 7A and C), supporting the worsened behavioral phenotypes observed in R6/2 ENT3<sup>-/-</sup> mice. Moreover, a considerable presence of TUNEL<sup>+</sup> cells was observed in the R6/2 ENT3<sup>-/-</sup> striatum (Fig. 7B and D), echoing the R6/2 ENT3<sup>-/-</sup> microglial defects and their failure to clean apoptotic

cells. The damaged mature neurons and the accumulation of dead cells in the striatum are highly likely to impact brain physiology. Since the brain is the most energy-consuming organ in the body, we speculated that R6/2 ENT3<sup>-/-</sup> mice might experience a disturbance in brain energy homeostasis. Defects in energy generation have been observed in HD patients with various proposed cellular mechanisms (Mochel & Haller, 2011), underlining the importance of energy flow in the brain to maintain its function. Having observed the lysosomal defects together with the mitochondrial accumulation phenotype, we speculated that abnormal mitophagy instead of increased mitogenesis was a plausible explanation. Mitophagy can be initiated via multiple pathways, including the PINK1/Parkin pathway (Wang et al., 2023; Yao et al., 2024). While ENT3 deficiency disturbs lysosomal functions, it is unclear if the PINK1/Parkin pathway is impacted. To address this question, we harvested striatal tissues for western blot analysis to evaluate the PINK1 and Parkin levels in R6/2 ENT3<sup>-/-</sup> mice. Although no differences were found at the PINK1 level, an apparent accumulation of Parkin was observed in R6/2 ENT3<sup>-/-</sup> mice (Fig. 7E-G), agreeing with the elevated MitoTracker signals (Fig. 5F) and arguing for the defective mitophagy in these animals. We applied the extracellular flux assay with live brain slices to obtain a real-time evaluation of the energy generation process. While no significant differences were identified in oxygen consumption rate (OCR) between WT and ENT3 $^{-/-}$  striatum (Fig. 7H), we noted that R6/2 ENT3<sup>-/-</sup> striatum showed decreased OCR compared to R6/2 littermates (Fig. 7I). When examined in detail, we found that R6/2 striatum had elevated basal respiration (Fig. 7J), ATP production (Fig. 7K), and maximal respiration (Fig. 7L) comparing to WT littermates, suggesting a higher demand for energy generation to cope with the HDassociated stress. These results also implied that although the HD brain has a general energy deficit, it actively compensates for the shortage by activating the mitochondrial energy production pathway. However, this rescue response is obliterated in the absence of ENT3, suggesting that ENT3 belongs to the module that supports the extra energy generation demand upon HD challenge, and the lack of ENT3 exacerbates the progression of HD. To obtain a more comprehensive energy generation profile, we further measured the usage of glycolysis in these brain sections at basal (Supplemental Fig. 3A) or stress respiration (Supplemental Fig. 3B) states. The analyses showed that R6/2 brain samples are prone to the usage of mitochondrial oxidative phosphorylation to generate energy, and the deficiency of ENT3 impacted this rescue response under R6/2 setting. These results collectively demonstrated that ENT3 participates in supplementing the extra brain energy generation demand in the HD-like R6/2 brain.

#### 4. Discussion

As nucleoside transporters that maintain the equilibrium of extraand intra-cellular nucleosides and nucleotides, ENTs have drawn attention primarily to their vital roles in transporting nucleoside analogs in cancer therapy. However, more knowledge is required to know about their contribution in different disease settings. It has recently been suggested that adjusting adenosine tone by targeting ENT1 can be a potential therapeutic measure for neurodegenerative diseases such as HD (Kao et al., 2017) or Alzheimer's disease (Lee et al., 2018) and that the deletion of ENT2 worsens HD progression in a mouse model (Chen et al., 2023), highlighting the involvement of ENTs in the brain. Notably,



(caption on next page)

Fig. 6. Deficiency of ENT3 leads to microglial dysfunctions in R6/2 ENT3 $^{-/-}$ . (A)The lysosomal membrane permeability in microglia was evaluated by Galectin-3 and Iba-1 immunofluorescent staining of brain tissue sections. Scale bars = 20  $\mu$ m. Three fields were taken for every section; three sections were collected and quantified per mouse. Quantification of Galectin-3 signals (N = 4–8) (B) and Iba-1 (N = 7–10) (C) were performed. (D) Brain tissue sections from R6/2 ENT3 $^{+/+}$  and R6/2 ENT3 $^{-/-}$  mice were stained with EM48, CD68, and Iba-1 to assess the microglial function. Scale bar = 50  $\mu$ m, and 20  $\mu$ m for the inlets. Representative images from 3 independent experiments were shown. (E) Workflow of primary microglia degradation assay. (F) The degradation index was calculated by enumerating the GFP $^+$  microglia/field (%) and shown in the violin plot (n = 18, combined results from two independent experiments). All values were shown as mean  $\pm$  SEM. Statistical analyses were performed with unpaired t-tests. t0.005, t0.01, or labeled on the graphs.

the distinct localization of ENTs imposes differential biological functions – while both ENT1 and ENT2 are membrane-targeting transporters that modulate the nucleoside dynamics between the cell and its residing microenvironment, the current study on the endosomal/lysosomal ENT3 reveals the importance of intracellular nucleoside balance mediated by ENT3 and its protective role under HD setting.

It is known that mHTT aggregates lead to a cascade of events that disrupt metabolism, including the downregulation of peroxisome proliferator-activated receptor-g (PPARg) (Chiang et al., 2010), disturbance in AMPK-a1 activity (Ju et al., 2011), and dysfunction of mitochondria (Dai et al., 2023). As any compromise in energy production or utilization can have profound consequences in the brain, it is unsurprising that the affected brain would trigger compensatory measures before irreversible damage occurs. However, how the HD-affected brain responds and copes with the energy crisis is still being determined. The seahorse experiment was done with live brain sections to provide an overview of the brain energy flow in these mice. Interestingly, we found that R6/2 ENT3<sup>+/+</sup> mice have significantly higher OCR compared to WT controls, yet this elevation of OCR was not observed in R6/2 ENT3<sup>-/-</sup> (Fig. 7J-L). We speculate the elevated OCR usage in R6/2 ENT3<sup>+/+</sup> is likely a rescue response – in the presence of neural death (Fig. 7A and C), the residual cells need to generate more energy through mitochondrial oxidative phosphorylation (Fig. 7I-L, Supplemental Fig. 3), a metabolic response that relies heavily on maintaining a functional and healthy mitochondria pool. However, the absence of ENT3 impacts mitophagy (Fig. 7E-G), thus hindering this compensatory response. The lack of this energy boost in R6/2 ENT3<sup>-/-</sup> leaves these mice in an energy-deficit state, likely reflecting their progressed HD-like phenotypes. Our study suggests that ENT3-mediated metabolism is an integral part of HD's compensatory energy generation module. In the absence of ENT3, the HD brain experiences difficulties utilizing the mitochondrial reserve to overcome energy insufficiency. Together, these results suggest that deficiency of ENT3 results in metabolic derangements, which can exacerbate the physical and cognitive symptoms of the disease.

While ENT3 has been reported to have a mitochondrial localization (Liu et al., 2015), it is still unclear how or if ENT3 supports mitochondria function (Huber-Ruano et al., 2012). We propose that ENT3, at least in part, influences mitochondrial activities indirectly via participating in mitophagy, the cellular machinery to adjust mitochondria function and maintain the health of the mitochondria pool, based on the observations of mitochondria accumulation and the elevation of cellular ROS in the R6/2 ENT3 $^{-/-}$  microglia. However, we could not rule out the possible contribution of mitochondrial ENT3-mediated nucleoside translocation in regulating mitochondria activities under the HD disease setting. Whether ENT3 exerts its protective function in HD via mediating intraorganelle nucleoside balance or supporting lysosomal functions awaits further investigation.

As one of the autophagic processes, mitophagy relies on lysosomes. Lysosomes are acidic organelles in most cells, including neurons, astrocytes, and microglia, and are known as a pivotal cellular waste disposal system. It is becoming clear that lysosomes are also the cell's recycling center, breaking down cellular waste and recycling materials, which helps maintain cellular homeostasis. Although HD is traditionally considered a genetic disorder, the role of lysosomes in the pathogenesis of HD has gained increasing attention in recent years due to its activity in the clearance of cellular debris and misfolded proteins. In HD, the mHTT tends to aggregate and form toxic clumps, which can overwhelm the lysosomal degradation machinery. This leads to impaired lysosomal

function and the buildup of toxic protein aggregates within neurons, which eventuates neuronal dysfunction and death. As the professional scavenger and the primary surveillance system in the brain, microglia receive these environmental cues and act to reclaim the balance state. In the presence of mHTT aggregates and damaged/dead neurons, microglia respond by phagocytosing these biomaterials and initiating the consequent activations. Since we observed that in both the HD-mouse model and patients (Fig. 4), the presence of mHTT aggregates correlates with the ENT3 expression, we reasoned that these degradation demands cue for the lysosome biogenesis, which includes the synthesis of lysosomal membrane proteins (Yang & Wang, 2021) such as ENT3 to support the lysosomal function.

Mitophagy can be initiated through multiple mechanisms, including PINK1/Parkin-dependent and independent pathways (Wang et al., 2023). mHTT protein has been shown to result in the dysfunction of mitochondrial homeostasis and impaired mitophagy (Quinn et al., 2020), and the overexpression of PINK1 generates a neuroprotective effect in HD (Khalil et al., 2015). While ENT3 deficiency disturbs lysosomal functions, if it has a direct impact on the PINK1/Parkin pathway is unclear. The striatal tissue of R6/2 ENT3<sup>-/-</sup> showed no significant difference in PINK1 level compared to control groups but had a substantial accumulation of Parkin (Fig. 7E-G). These results suggest that the PINK1/Parkin axis is affected in R6/2 ENT3<sup>-/-</sup>. Although the PINK1 machinery remains normal without ENT3, the inefficient autophagosome degradation of aged/damaged mitochondria led to the accumulation of Parkin in R6/2 ENT3<sup>-/-</sup>, agreeing with the elevated MitoTracker signals (Fig. 5F), yet defective mitochondrial function in R6/2 ENT3<sup>-/-</sup> (Fig. 7J-K). Although controversies exist, emerging studies using several HD models suggest that mHTT affects multiple steps in the mitophagy pathway (Li et al., 2023). Our results position ENT3, a lysosomal metabolite transporter, as part of this complex machinery. Further experiments are needed to understand the detailed mechanism and the contribution of ENT3 in the process.

In neurodegenerative diseases like HD, microglia activation plays a complex role – it can lead to either beneficial or detrimental outcomes depending on the disease stages (Yang et al., 2017; Savage et al., 2020). Loss-of-function of ENT3 drives histiocytosis has been demonstrated in multiple studies. While phagocyte accumulation under ENT3 deficiency has been explained by the over-activation of M-CSF/M-CSFR and TLR7/ 8-MAPK signaling axes (Hsu et al., 2012; Shiloh et al., 2023) (Shibata et al., 2023), it is noteworthy that these nucleoside-ladened myeloid cells, including monocytes, splenic macrophages, as well as microglia, do not have active inflammatory phenotypes (Fig. 2D and E). Moreover, these  $\mathrm{ENT3}^{-/-}$  microglia had higher production of immunosuppressive effectors such as IL-10 and Arginase-1 (Fig. 3D and E). However, it was unknown if the expression of ENT3 in microglia is an ally or foe for HD progression. The results with genetic models strongly (Fig. 4I and J) suggest that the upregulation of ENT3 during HD progression (Fig. 4A-F) is a protective response, likely to compensate for the intensified demand to remove protein aggregates and cellular debris.

The potential for modulating microglial function to treat HD has recently gained significant attention. Various approaches, including small molecules, gene therapy, and immunomodulatory agents, are being explored to target microglia and reduce their pro-inflammatory responses. Some of these approaches aim to dampen microglial activation, while others focus on enhancing their phagocytic capacity to remove mHTT aggregates. Moreover, the presence of Galectin-3 positive signals in microglia under the condition of ENT3 deficiency and mHTT

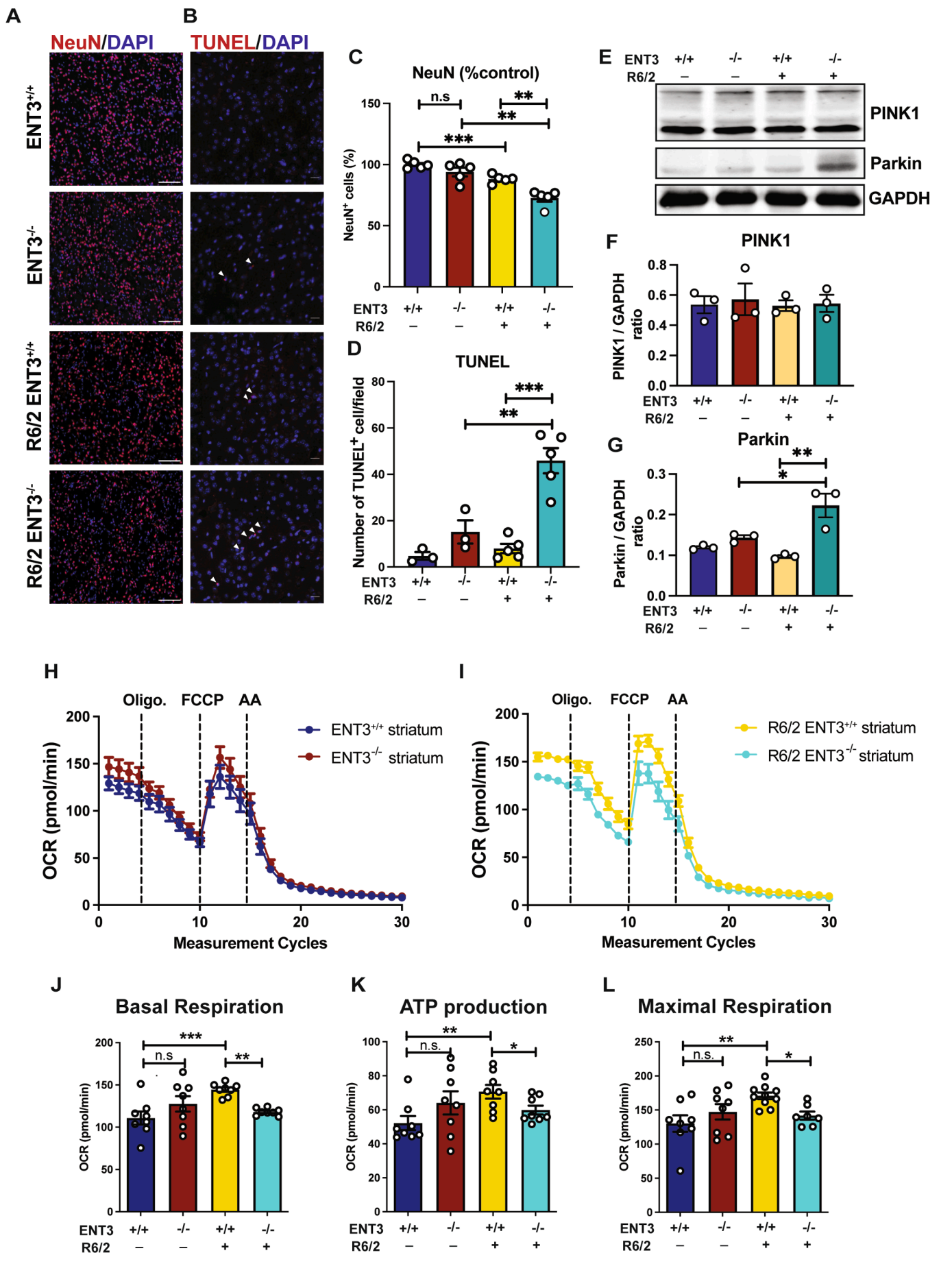


Fig. 7. ENT3 is involved in the brain's homeostasis and energy balance. (A) Mature neurons in the striatum were measured by NeuN immunofluorescence staining of brain tissue sections and were analyzed with ImageJ (N = 5). Scale bars = 100  $\mu$ m. (B) The presence of apoptotic cells in the striatum was detected by TUNEL assay immunofluorescence staining of brain tissue sections and analyzed with IMARIS (N = 3–5). Scale bars = 50  $\mu$ m. The quantification of NeuN (C) or TUNEL (D) signals was shown in NeuN<sup>+</sup> cells/DAPI<sup>+</sup> field (%) or TUNEL<sup>+</sup> cell/field (number), respectively. (E) The activation of mitophagy-associated machinery was evaluated by examining the expression of PINK1 and Parkin. The quantification of PINK1 (F) and Parkin (G) was shown by its ratio to GAPDH (N = 3). The oxygen consumption rate (OCR) of live striatal tissue of ENT3<sup>-/-</sup> and littermates (H) or R6/2 ENT3<sup>+/+</sup> and R6/2 ENT3<sup>-/-</sup> (I) was measured by extracellular flux assay using the Seahorse analyzer. The basal respiration (J), ATP production (K), and maximal respiration (L) measurements were quantified. The preferential usage of glycolysis vs. oxidative phosphorylation was evaluated by comparing the extracellular acidification rate (ECAR) and OCR (N = 8). All values were shown as mean  $\pm$  SEM. Statistical analyses were performed with unpaired *t*-tests. \*p < 0.05, \*\*p < 0.01, \*\*\*p < 0.001, n.s. not significant.

accumulation suggests that ENT3 helps to maintain the lysosomal integrity while mHTT aggregates break it (Fig. 6A and B). Siew et al. recently suggested that Galectin-3 may aggravate microglial activation (Siew et al., 2023) further highlighting the understanding that these lysosomal mechanisms can offer potential therapeutic targets for HD by promoting the clearance of toxic mHTT aggregates and attenuating undesirable microglial activation. Developing therapies that modulate microglial function, shifting the balance toward a more protective and anti-inflammatory phenotype, could slow the progression of HD and alleviate its symptoms.

What molecular and cellular mechanisms govern the communication between neurons and microglia in Huntington's disease? How do microglia respond to signals from degenerating neurons, and how does this crosstalk contribute to disease progression or, potentially, neuroprotection? This study shows that the interaction between microglia and neurons seems direct and intimate. Although ENT3 mainly functions within microglia, its deficiency results in increased neuron death as well as the accumulation of apoptotic cells in the brain (Fig. 7A and B). These results imply that ENT3 may have a role in the microglial-associated neuroprotection, although the detailed molecular mechanism needs further investigation. Microglia interact with other neurons and brain cells, such as astrocytes, in a complex network. Astrocytes, another type of glial cell in the brain, provide metabolic support to neurons. Microglia can influence astrocyte function (Matejuk & Ransohoff, 2020), and the disruptions in this relationship can affect neuronal energy metabolism, potentially exacerbating HD-related metabolic disturbances.

### 5. Conclusions

The relationship between Huntington's disease and microglia is complex, with these immune cells playing both protective and detrimental roles in the pathogenesis of the disease. Understanding the dynamics of microglia activation, their interactions with other brain cells, and their potential for modulatory therapies is crucial for developing effective treatments for HD. This study identifies that the microglial metabolite transporter, ENT3, has a protective role in HD-associated crises. Research in this area offers hope for the development of interventions that may slow the progression of the disease, mitigate its symptoms, and ultimately improve the quality of life for individuals and families affected by Huntington's disease.

### CRediT authorship contribution statement

Ying-Sui Lu: Visualization, Investigation, Data curation. Wei-Chien Hung: Methodology, Investigation. Yu-Ting Hsieh: Methodology, Investigation. Pei-Yuan Tsai: Methodology, Investigation. Tsai-Hsien Tsai: Investigation. Hsiu-Han Fan: Investigation. Ya-Gin Chang: Investigation. Hui-Kuei Cheng: Investigation. Shen-Yan Huang: Investigation. Hsin-Chuan Lin: Investigation. Yan-Hua Lee: Investigation. Tzu-Hsiang Shen: Investigation. Bing-Yu Hung: Investigation. Jin-Wu Tsai: Methodology. Ivan Dzhagalov: Writing – review & editing, Supervision, Methodology, Conceptualization. Irene Han-Juo Cheng: Methodology. Chun-Jung Lin: Resources, Methodology, Funding acquisition, Conceptualization. Yijuang Chern: Resources, Methodology, Funding acquisition, Data curation, Conceptualization. Chia-Lin Hsu: Writing – review & editing, Writing – original draft,

Supervision, Resources, Project administration, Investigation, Formal analysis, Data curation, Conceptualization.

#### **Declaration of competing interest**

The authors declare that they have no known competing financial interests or personal relationships that could have appeared to influence the work reported in this paper.

#### Data availability

Data will be made available on request.

### Acknowledgment

We thank the Taiwan Mouse Clinic for performing the modified SHIRPA experiment and the Laboratory Animal Center of National Yang Ming Chiao Tung University for animal keeping. We thank Dr. Manikandan Narayanan (Robert Bosch Center for Data Science and AI, IIT, In) for generously sharing the microarray data previously published (Narayanan et al., 2014) and appreciate the support from Dr. Ching-Pang Chang at IBMS Academia Sinica for processing the microarray data. We thank Dr. Shu-Jung Chang (NTU) and Dr. Wei-Chung Chiang (NYCU) for the useful discussion and the sharing of antibodies. Leo Dzhagalov helped to proofread this manuscript. Behavioral studies were carried out at the Animal Behavioral Core supported by the Brain Research Center NYCU, from The Featured Areas Research Center Program within the Higher Education Sprout Project framework by the Ministry of Education in Taiwan (MOE). This work is funded by NSTC 107-2320-B-010-020, 108-2320-B-010-003, 109-2320-B-010-046, 110-2320-B-001-011, 112-2321-B-001-008 and Cancer Progression Research Center NYCU to C.-L. Hsu.

### Appendix A. Supplementary data

Supplementary data to this article can be found online at https://doi. org/10.1016/j.bbi.2024.06.021.

## References

Aartsma-Rus, A., van Putten, M., 2014. Assessing functional performance in the mdx mouse model. J. Vis. Exp. 85, 51303. https://doi.org/10.3791/51303.

Aits, S., Kricker, J., Liu, B., Ellegaard, A.M., Hämälistö, S., Tvingsholm, S., Corcelle-Termeau, E., Høgh, S., Farkas, T., Holm Jonassen, A., Gromova, I., Mortensen, M., Jäättelä, M., 2015. Sensitive detection of lysosomal membrane permeabilization by lysosomal galectin puncta assay. Autophagy 11 (8), 1408–1424. https://doi.org/10.1080/15548627.2015.1063871.

Bloom, J.L., Lin, C., Imundo, L., Guthery, S., Stepenaskie, S., Galambos, C., Lowichik, A., Bohnsack, J.F., 2017. H syndrome: 5 new cases from the United States with novel features and responses to therapy. Pediatr. Rheumatol. Online J. 15 (1), 76. https://doi.org/10.1186/s12969-017-0204-y.

Chen, C.Y., Chou, F.Y., Chang, Y.G., Ho, C.J., Wu, K.C., Hsu, C.L., Chern, Y., Lin, C.J., 2023. Deletion of equilibrative nucleoside transporter 2 disturbs energy metabolism and exacerbates disease progression in an experimental model of Huntington's disease. Neurobiol. Dis. 177, 106004 https://doi.org/10.1016/j.nbd.2023.106004.

Chiang, M.C., Chen, C.M., Lee, M.R., Chen, H.W., Chen, H.M., Wu, Y.S., Hung, C.H., Kang, J.J., Chang, C.P., Chang, C., Wu, Y.R., Tsai, Y.S., Chern, Y., 2010. Modulation of energy deficiency in Huntington's disease via activation of the peroxisome proliferator-activated receptor gamma. Hum. Mol. Genet. 19 (20), 4043–4058. https://doi.org/10.1093/hmg/ddq322.

- Chistiakov, D.A., Killingsworth, M.C., Myasoedova, V.A., Orekhov, A.N., Bobryshev, Y. V., 2017. CD68/macrosialin: not just a histochemical marker. Lab. Invest. 97 (1), 4–13. https://doi.org/10.1038/labinvest.2016.116.
- Colonna, M., Butovsky, O., 2017. Microglia function in the central nervous system during health and neurodegeneration. Annu. Rev. Immunol. 35, 441–468. https://doi.org/ 10.1146/annurev-immunol-051116-052358.
- Dai, Y., Wang, H., Lian, A., Li, J., Zhao, G., Hu, S., Li, B., 2023. A comprehensive perspective of Huntington's disease and mitochondrial dysfunction. Mitochondrion 70, 8–19. https://doi.org/10.1016/j.mito.2023.03.001.
- Dubinsky, J.M., 2017. Towards an understanding of energy impairment in Huntington's disease brain. J. Huntingtons Dis. 6 (4), 267–302. https://doi.org/10.3233/JHD-170264
- Gao, C., Jiang, J., Tan, Y., Chen, S., 2023. Microglia in neurodegenerative diseases: mechanism and potential therapeutic targets. Signal Transduct. Target. Ther. 8 (1), 359. https://doi.org/10.1038/s41392-023-01588-0.
- Hong, S.L., Cossyleon, D., Hussain, W.A., Walker, L.J., Barton, S.J., Rebec, G.V., 2012. Dysfunctional behavioral modulation of corticostriatal communication in the R6/2 mouse model of Huntington's disease. PLoS One 7 (10), e47026.
- Hsu, C.L., Lin, W., Seshasayee, D., Chen, Y.H., Ding, X., Lin, Z., Suto, E., Huang, Z., Lee, W.P., Park, H., Xu, M., Sun, M., Rangell, L., Lutman, J.L., Ulufatu, S., Stefanich, E., Chalouni, C., Sagolla, M., Diehl, L., Martin, F., 2012. Equilibrative nucleoside transporter 3 deficiency perturbs lysosome function and macrophage homeostasis. Science 335 (6064), 89–92. https://doi.org/10.1126/science.1213682.
- Huber-Ruano, I., Errasti-Murugarren, E., Godoy, V., Vera, Á., Andreu, A.L., Garcia-Arumi, E., Martí, R., Pastor-Anglada, M., 2012. Functional outcome of a novel SLC29A3 mutation identified in a patient with H syndrome. Biochem. Biophys. Res. Commun. 428 (4), 532–537. https://doi.org/10.1016/j.bbrc.2012.09.143.
- Jimenez-Sanchez, M., Licitra, F., Underwood, B.R., Rubinsztein, D.C., 2017. Huntington's disease: mechanisms of pathogenesis and therapeutic strategies. Cold Spring Harb. Perspect. Med. 7 (7), a024240 https://doi.org/10.1101/cshperspect. a024240.
- Ju, T.C., Chen, H.M., Lin, J.T., Chang, C.P., Chang, W.C., Kang, J.J., Sun, C.P., Tao, M.H., Tu, P.H., Chang, C., Dickson, D.W., Chern, Y., 2011. Nuclear translocation of AMPKalpha1 potentiates striatal neurodegeneration in Huntington's disease. J. Cell Biol. 194 (2), 209–227. https://doi.org/10.1083/jcb.201105010.
- Kao, Y.H., Lin, M.S., Chen, C.M., Wu, Y.R., Chen, H.M., Lai, H.L., Chern, Y., Lin, C.J., 2017. Targeting ENT1 and adenosine tone for the treatment of Huntington's disease. Hum. Mol. Genet. 26 (3), 467–478. https://doi.org/10.1093/hmg/ddw402.
- Khalil, B., El Fissi, N., Aouane, A., Cabirol-Pol, M.J., Rival, T., Liévens, J.C., 2015. PINK1-induced mitophagy promotes neuroprotection in Huntington's disease. Cell Death Dis. 6 (1), e1617.
- Lee, C.C., Chang, C.P., Lin, C.J., Lai, H.L., Kao, Y.H., Cheng, S.J., Chen, H.M., Liao, Y.P., Faivre, E., Buée, L., Blum, D., Fang, J.M., Chern, Y., 2018. Adenosine augmentation evoked by an ENT1 inhibitor improves memory impairment and neuronal plasticity in the APP/PS1 mouse model of Alzheimer's disease. Mol. Neurobiol. 55 (12), 8936–8952. https://doi.org/10.1007/s12035-018-1030-z.
- Lee, Z.F., Huang, T.H., Chen, S.P., Cheng, I.H., 2021. Altered nociception in Alzheimer disease is associated with striatal-enriched protein tyrosine phosphatase signaling. Pain 162 (6), 1669–1680. https://doi.org/10.1097/j.pain.000000000002180.
- Pain 162 (6), 1669–1680. https://doi.org/10.1097/j.pain.00000000000002180. Lee, Y.H., Tsai, Y.S., Chang, C.C., Ho, C.C., Shih, H.M., Chen, H.M., Lai, H.L., Lee, C.W., Lee, Y.C., Liao, Y.C., Yang, U.C., Cheng, T.H., Chern, Y., Soong, B.W., 2022. A PIAS1 protective variant S510G delays polyQ disease onset by modifying protein homeostasis. Mov. Disord. 37 (4), 767–777. https://doi.org/10.1002/mds.28896.
- Li, J., Yang, D., Li, Z., Zhao, M., Wang, D., Sun, Z., Wen, P., Dai, Y., Gou, F., Ji, Y., Zhao, D., Yang, L., 2023. PINK1/Parkin-mediated mitophagy in neurodegenerative diseases. Ageing Res. Rev. 84, 101817 https://doi.org/10.1016/j.arr.2022.101817.
- Liu, Y.L., Chen, W.T., Lin, Y.Y., Lu, P.H., Hsieh, S.L., Cheng, I.H., 2017. Amelioration of amyloid-β-induced deficits by DcR3 in an Alzheimer's disease model. Mol. Neurodegener. 12 (1), 30. https://doi.org/10.1186/s13024-017-0173-0.
- Liu, B., Czajka, A., Malik, A.N., Hussain, K., Jones, P.M., Persaud, S.J., 2015. Equilibrative nucleoside transporter 3 depletion in  $\beta$ -cells impairs mitochondrial function and promotes apoptosis: relationship to pigmented hypertrichotic dermatosis with insulin-dependent diabetes. BBA 1852 (10 Pt A), 2086–2095. https://doi.org/10.1016/j.bbadis.2015.07.002.
- Lukens, J.R., Eyo, U.B., 2022. Microglia and neurodevelopmental disorders. Annu. Rev. Neurosci. 45, 425–445. https://doi.org/10.1146/annurev-neuro-110920-023056.
- Ma, H., Qu, J., Liao, Y., Liu, L., Yan, M., Wei, Y., Xu, W., Luo, J., Dai, Y., Pang, Z., Qu, Q., 2023. Equilibrative nucleotide transporter ENT3 (SLC29A3): a unique transporter for inherited disorders and cancers. Exp. Cell Res. 434 (2), 113892 https://doi.org/10.1016/j.vexcr.2023.113892.
- Masuya, H., Inoue, M., Wada, Y., Shimizu, A., Nagano, J., Kawai, A., Inoue, A., Kagami, T., Hirayama, T., Yamaga, A., Kaneda, H., Kobayashi, K., Minowa, O., Miura, I., Gondo, Y., Noda, T., Wakana, S., Shiroishi, T., 2005. Implementation of the modified-SHIRPA protocol for screening of dominant phenotypes in a large-scale ENU mutagenesis program. Mamm. Genome 16 (11), 829–837. https://doi.org/10.1007/s00335-005-2430-8.
- Matejuk, A., Ransohoff, R.M., 2020. Crosstalk between astrocytes and microglia: an overview. Front. Immunol. 11, 1416. https://doi.org/10.3389/fimmu.2020.01416.

- Mochel, F., Haller, R.G., 2011. Energy deficit in Huntington disease: why it matters. J. Clin. Invest. 121 (2), 493–499. https://doi.org/10.1172/JCI45691.
- Muzio, L., Viotti, A., Martino, G., 2021. Microglia in neuroinflammation and neurodegeneration: from understanding to therapy. Front. Neurosci. 15, 742065 https://doi.org/10.3389/fnins.2021.742065.
- Narayanan, M., Huynh, J.L., Wang, K., Yang, X., Yoo, S., McElwee, J., Zhang, B., Zhang, C., Lamb, J.R., Xie, T., Suver, C., Molony, C., Melquist, S., Johnson, A.D., Fan, G., Stone, D.J., Schadt, E.E., Casaccia, P., Emilsson, V., Zhu, J., 2014. Common dysregulation network in the human prefrontal cortex underlies two neurodegenerative diseases. Mol. Syst. Biol. 10 (7), 743. https://doi.org/10.15252/msb.20145304.
- Palpagama, T.H., Waldvogel, H.J., Faull, R.L.M., Kwakowsky, A., 2019. The role of microglia and astrocytes in Huntington's disease. Front. Mol. Neurosci. 12, 258. https://doi.org/10.3389/fnmol.2019.00258.
- Platt, F.M., Boland, B., van der Spoel, A.C., 2012. The cell biology of disease: lysosomal storage disorders: the cellular impact of lysosomal dysfunction. J. Cell Biol. 199 (5), 723–734. https://doi.org/10.1083/jcb.201208152.
- Qi, G., Mi, Y., Yin, F., 2021. Characterizing brain metabolic function ex vivo with acute mouse slice punches. STAR Protoc 2 (2), 100559. https://doi.org/10.1016/j. xxxx 2021 100559
- Quinn, P.M.J., Moreira, P.I., Ambrósio, A.F., Alves, C.H., 2020. PINK1/PARKIN signalling in neurodegeneration and neuroinflammation. Acta Neuropathol. Commun. 8 (1), 189. https://doi.org/10.1186/s40478-020-01062-w.
- Sapp, E., Kegel, K.B., Aronin, N., Hashikawa, T., Uchiyama, Y., Tohyama, K., Bhide, P.G., Vonsattel, J.P., DiFiglia, M., 2001. Early and progressive accumulation of reactive microglia in the Huntington disease brain. J. Neuropathol. Exp. Neurol. 60 (2), 161–172. https://academic.oup.com/jnen/article/60/2/161/2610064.
- Savage, J.C., St-Pierre, M.K., Carrier, M., El Hajj, H., Novak, S.W., Sanchez, M.G., Cicchetti, F., Tremblay, M.E., 2020. Microglial physiological properties and interactions with synapses are altered at presymptomatic stages in a mouse model of Huntington's disease pathology. J. Neuroinflammation 17 (1), 98. https://doi.org/ 10.1186/s12974-020-01782-9.
- Shibata, T., Sato, R., Taoka, M., Saitoh, S.I., Komine, M., Yamaguchi, K., Goyama, S., Motoi, Y., Kitaura, J., Izawa, K., Yamauchi, Y., Tsukamoto, Y., Ichinohe, T., Fujita, E., Hiranuma, R., Fukui, R., Furukawa, Y., Kitamura, T., Takai, T., Miyake, K., 2023. TLR7/8 stress response drives histiocytosis in SLC29A3 disorders. J. Exp. Med. 220 (9), e20230054.
- Shiloh, R., Lubin, R., David, O., Geron, I., Okon, E., Hazan, I., Zaliova, M., Amarilyo, G., Birger, Y., Borovitz, Y., Brik, D., Broides, A., Cohen-Kedar, S., Harel, L., Kristal, E., Kozlova, D., Ling, G., Shapira Rootman, M., Shefer Averbuch, N., Elitzur, S., 2023.
  Loss of function of ENT3 drives histiocytosis and inflammation through TLR-MAPK signaling. Blood 142 (20). 1740–1751. https://doi.org/10.1182/blood.2023020714.
- Siew, J.J., Chen, H.M., Chiu, F.L., Lee, C.W., Chang, Y.M., Chen, H.L., Nguyen, T.N.A., Liao, H.T., Liu, M., Hagar, H.T., Sun, Y.C., Lai, H.L., Kuo, M.H., Blum, D., Buée, L., Jin, L.W., Chen, S.Y., Ko, T.M., Huang, J.R., Chern, Y., 2023. Galectin-3 aggravates microglial activation and tau transmission in tauopathy. J. Clin. Invest. e165523 https://doi.org/10.1172/JCI165523.
- Tabrizi, S.J., Flower, M.D., Ross, C.A., Wild, E.J., 2020. Huntington disease: new insights into molecular pathogenesis and therapeutic opportunities. Nat. Rev. Neurol. 16 (10), 529–546. https://doi.org/10.1038/s41582-020-0389-4.
- Tang, T., Li, L., Tang, J., Li, Y., Lin, W.Y., Martin, F., Grant, D., Solloway, M., Parker, L., Ye, W., Forrest, W., Ghilardi, N., Oravecz, T., Platt, K.A., Rice, D.S., Hansen, G.M., Abuin, A., Eberhart, D.E., Godowski, P., de Sauvage, F.J., 2010. A mouse knockout library for secreted and transmembrane proteins. Nat. Biotechnol. 28 (7), 749–755. https://doi.org/10.1038/nbt.1644.
- Wang, S., Long, H., Hou, L., Feng, B., Ma, Z., Wu, Y., Zeng, Y., Cai, J., Zhang, D.W., Zhao, G., 2023. The mitophagy pathway and its implications in human diseases. Signal Transduct. Target. Ther. 8 (1), 304. https://doi.org/10.1038/s41392-023-01503-7.
- Wei, C.W., Lee, C.Y., Lee, D.J., Chu, C.F., Wang, J.C., Wang, T.C., Jane, W.N., Chang, Z. F., Leu, C.M., Dzhagalov, I.L., Hsu, C.L., 2018. Equilibrative nucleoside transporter 3 regulates T cell homeostasis by coordinating lysosomal function with nucleoside availability. Cell Rep. 23 (8), 2330–2341. https://doi.org/10.1016/j.celrep.2018.04.077.
- Wilton, D.K., Stevens, B., 2020. The contribution of glial cells to Huntington's disease pathogenesis. Neurobiol. Dis. 143, 104963 https://doi.org/10.1016/j. nbd.2020.104963.
- Yang, C., Wang, X., 2021. Lysosome biogenesis: regulation and functions. J. Cell Biol. 220 (6), e202102001.
- Yang, H.M., Yang, S., Huang, S.S., Tang, B.S., Guo, J.F., 2017. Microglial activation in the pathogenesis of Huntington's disease. Front. Aging Neurosci. 9, 193. https://doi. org/10.3389/fnagi.2017.00193.
- Yao, J., Kan, B., Dong, Z., Tang, Z., 2024. Research progress of mitophagy in Alzheimer's disease. Curr. Alzheimer Res. https://doi.org/10.2174/ 0115672050300063240305074310.
- Zhao, T., Hong, Y., Li, X.J., Li, S.H., 2016. Subcellular clearance and accumulation of Huntington disease protein: a mini-review. Front. Mol. Neurosci. 9, 27. https://doi. org/10.3389/fnmol.2016.00027.